Surface and Electronic Features of Fluorinated TiO 2 and Their Influence on the Photocatalytic Degradation of 1-Methylnaphthalene

Nidhal Fessi, Mohamed Faouzi Nsib, Luis Cardenas, Chantal Guillard, Frederic Dappozze, Ammar Houas, Francesco Parrino, Leonardo Palmisano, Gilles Ledoux, David Amans, et al.

Surface and Electronic Features of Fluorinated TiO_2 and their Influence on the Photocatalytic Degradation of 1-Methylnaphthalene

Nidhal Fessi,[a,b] Mohamed Faouzi Nsib,[a,g] Luis Cardenas,[c] Chantal Guillard,[c] Frédéric Dappozze,[c] Ammar Houas,[a] Francesco Parrino,[*,d] Leonardo Palmisano,[e] Gilles Ledoux,[f] David Amans,[f] Yves Chevalier[*,b]

[a] Laboratoire de Recherche Catalyse et Matériaux pour l'Environnement et les Procédés (URCMEP, UR11ES85), Faculté des Sciences de Gabès, University of Gabès, Campus Universitaire, Cité Erriadh, 6072 Gabès, Tunisia.

[b] Laboratoire d'Automatique, de Génie des Procédés et de Génie Pharmaceutique (LAGEPP), CNRS UMR 5007, University Claude Bernard Lyon 1, 43 bd 11 Novembre, 69622 Villeurbanne, France.

[c] Institut de Recherches sur la Catalyse et l'Environnement de Lyon (IRCELYON), CNRS UMR 5256, Université Lyon 1, 2 av Albert Einstein, 69626 Villeurbanne, France.

[d] Industrial Engineering Department, University of Trento, via Sommarive 9, 38123 Trento, Italy.

[e] Department of Engineering, University of Palermo, Viale delle Scienze Ed. 6, 90128 Palermo, Italy.

[f] Université de Lyon, Université Claude Bernard Lyon 1, CNRS, Institut Lumière Matière, 69622 Villeurbanne, France.

[g] Higher School of Sciences and Technology of Hammam Sousse, University of Sousse, Tunisia.

*Correspondence: yves.chevalier@univ-lyon1.fr; francesco.parrino@unitn.it

Highlights.

- Surface fluorination of TiO_2 nanoparticles does not change their bulk structural properties
- Covalent binding through Ti–F bonds results from reaction of HF on TiO_2
- Defects coming from surface fluorination generate electronic states of energy levels in the band gap
- Energy levels of defects are close to the valence band

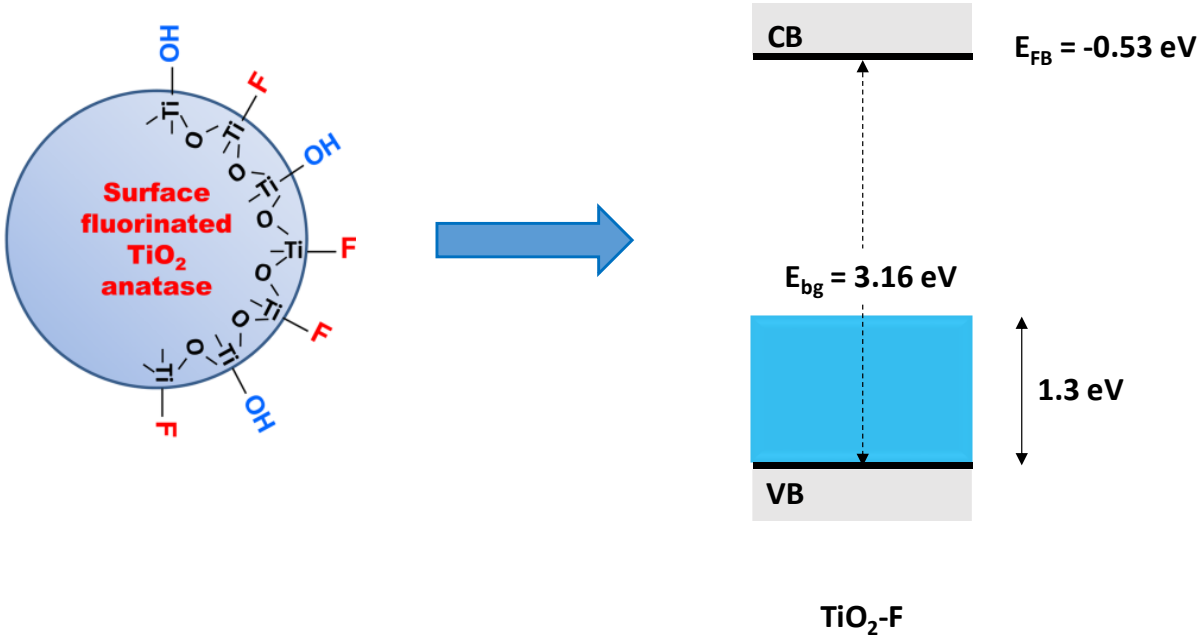

Abstract

Surface fluorination improves the photocatalytic activity of TiO_2 and the influences of various features of fluorinated TiO_2 (TiO_2-F) have often been discussed in the literature. The present paper addresses the changes induced by surface fluorination on the morphological, structural, surface and electronic features of TiO_2. In particular, X-ray diffraction, specific surface area analysis, and transmission and scanning electron microscopy give evidence that surface fluorination does not affect the structural properties and the morphology of TiO_2 nanoparticles. In contrast, fluorination induces changes of surface and electronic properties. Chemical and thermogravimetric analyses show that surface fluorination can reach up to 50% of original Ti–OH surface sites. The surface charge of TiO_2 turns more negative upon fluorination, as shown by a shift of the point of zero charge towards lower pH. Electronic properties are deeply characterized by combining diffuse reflectance, X-ray and UV photoelectron spectroscopies, as well as time-resolved fluorescence spectroscopy, and photo-electrochemical measurements. Results show the presence of intra band-gap energy states induced by the local interaction of chemisorbed fluorine atoms. Such energy levels are close to the valence band. The unique surface and electronic properties of TiO_2-F make it a promising material for the photocatalytic degradation of poorly soluble emerging pollutants such as 1-methylnaphtalene. In particular, TiO_2-F demonstrates faster degradation kinetics with respect to both the pristine material and TiO_2 P25 used as a benchmark standard.

Introduction

In the last decades, heterogeneous photocatalysis has been applied in different fields ranging from environmental remediation,[1–4] synthesis of high value added compounds,[5–7] self-cleaning surfaces,[8–11] dye-sensitized solar cells,[12,13] and photodynamic therapy[14,15] inter alia. TiO_2 is widely used as photocatalyst in most of these applications due to its high photoactivity, low cost, chemical inertness, photostability and "green" features.[16] UV light excitation of TiO_2 induces formation of photo-generated electrons (e_{cb}^-) and holes (h_{vb}^+) in the conduction and valence band, respectively.

The photogenerated charges, in turn, induce degradation of organic molecules (e.g. pollutants) in the surrounding liquid medium by direct interfacial electron transfer (IFET) or by indirect oxidation upon formation and release of highly oxidizing species[17] ($OH^\bullet$, $O_2^{\bullet-}$, H_2O_2, $NO_3^\bullet$) produced by interaction with oxygen and water.

However, despite the huge amount of papers published so far on environmental remediation by TiO_2 photocatalysis, large-scale applications for water treatment are hardly viable due to the large volume of effluents to be treated, and to the low reaction rates exhibited in the presence of highly concentrated pollutants. Coupling photocatalysis with other advanced oxidation processes can be an economically sustainable alternative due to the efficiency enhancement resulting from the synergy between the concomitant processes.[18–20] On another hand, photocatalysis alone can be competitive with traditional remediation processes for niche applications, such as the degradation of nearly insoluble pollutants in aqueous media downstream to physical separation plants. In fact, oil separation is a time demanding step in conventional plants and does not generally provide the required level of decontamination in reasonable treatment times. In this regard, it has been recently demonstrated that the degradation of insoluble pollutants in aqueous emulsions stabilized by bare TiO_2 is ca. 50 times faster than the degradation observed in biphasic systems.[21] This remarkable result is the starting point of the present investigation on surface fluorinated TiO_2 (TiO_2-F). The outstanding photocatalytic efficiency of TiO_2-F, reported in low concentrated pollutant solutions, along with its robust and stable features and facile preparation methods, make it a promising candidate for the degradation of poorly soluble pollutants in aqueous media. To this end, we deeply investigated the electronic and surface properties of TiO_2-F, responsible for its photocatalytic efficiency,

and tested its activity for the degradation of 1-methylnaphtalene, a recalcitrant polycyclic aromatic hydrocarbon.

Reaction of fluoride anions onto the TiO_2 surface results in substitution of hydroxyl groups with fluoride groups, yielding a TiO_2-F material bearing Ti–F species at its surface.[22] This strongly influences adsorption processes at the water–semiconductor interface, and remarkably affects the photocatalytic degradation of organic species depending on their affinity to the modified surface. As a result, the rate of photocatalytic degradations has been reported either to increase[23–27] or to decrease[28] for surface fluorinated TiO_2 with respect to the bare material. Among the various parameters affecting the photocatalytic activity, surface and electronic features are some of the most relevant.

As far as surface features are concerned, it is worth to mention that most of the molecules photocatalytically degraded in the presence of TiO_2-F so far reported, were soluble in water while less attention has been paid to the photodegradation of non-polar molecules. One example is the photodegradation of stearic acid in the presence of TiO_2-F catalyst.[26] However in this case, the photocatalyst and the substrate were separated by a thin air layer, in order to demonstrate the migration of the radical oxygen species which can behave as air-borne oxidants. For this reason, a part of this work is devoted to investigating the surface properties of TiO_2-F material and their influence on the degradation of non-polar pollutants.

With regards to electronic properties of TiO_2-F, it has been often reported that surface fluorination results in a selectively addressed interfacial electron transfer. For instance, Mrowetz and Selli[29] observed a higher hydroxyl radical production in the presence of TiO_2-F compared with bare TiO_2 and justified this result by considering the inhibited surface trapping of the photogenerated holes and the consequently more efficient hole induced direct water oxidation. In fact, surface fluorine groups enhance the Lewis acidity of the Ti^{4+} groups, which effectively adsorb molecular water.[30] Similarly, Minero et al.[23] reported faster photocatalytic degradation of phenol in the presence of surface modified TiO_2-F compared to pristine TiO_2 due to the enhanced formation of $OH^{\bullet}$ radicals. Maurino et al.[31] reported the sustained production of hydrogen peroxide (up to 1.3 mM) in the presence of TiO_2-F due to the competition of fluoride with superoxide/peroxide species at the surface of TiO_2 which consequently inhibited the degradation of the photogenerated

H_2O_2 which, therefore, accumulated in the system. However, the reported examples focus on electronic effects of the surface modification without any energetic characterization. As mentioned above, the enhanced photocatalytic activity has been mainly attributed to changes in the interfacial electron transfer path rather than to intrinsic energetic differences of the photogenerated charges. This conclusion has been justified by various experimental evidences. It is generally reported that the UV-vis spectrum of TiO_2-F does not show significant novel electronic transitions with respect to pristine TiO_2.[32] Moreover, the substitution of terminal –OH groups with isoelectronic –F ones does not produce variation of the charge balance, and the system is silent to highly sensitive techniques such as electron paramagnetic resonance.[33] X-ray photoelectron spectroscopy (XPS) enables the detection of surface fluorine atoms, but it is often not sensitive enough to retrieve information on possible electronic interactions between fluorine and TiO_2. On the other hand, UV photoelectron spectroscopy (UPS) is a more surface sensitive tool[34] that provides detailed information on the electronic density distribution of the valence band of semiconductive materials, which is not accessible by XPS owing to its low photoionization cross-section. This technique has been here applied for the first time to surface-fluorinated TiO_2 and highlighted the existence of intra band gap energy states close to the valence band of TiO_2.

The present investigation aims to correlate electronic and surface properties of the surface fluorinated TiO_2 with its activity towards the degradation of poorly soluble substrates dispersed in aqueous suspensions. 1-Methylnaphtalene (1-MN) has been used as a model pollutant to this aim. It is a widely used model for studying hazards of polycyclic aromatic hydrocarbons in environment.[35,36]

Experimental

Materials Synthesis and Reagents

TiO_2 nanoparticles were synthesized by using a simple sol-gel method.[37] In a typical synthesis, 19 mL of titanium tetraisopropoxide ($Ti[OCH(CH_3)_2]_4$ 97%, Alfa Aesar) were dissolved in 4 mL of methanol (MeOH 99.9%, Aldrich). The obtained solution was sonicated in an ultrasonic bath (Elma, T460/H, 35 kHz and 170 W). The hydrolysis process was then performed by adding dropwise 74 mL of deionized water under reflux

and magnetic stirring. After 3 h refluxing time, the obtained white gel was filtered and washed several times using ethanol and deionized water, dried at 100 °C for 18 h, and finally calcined at 400 °C for 4 h to obtain the pristine TiO_2 material, labelled below simply as TiO_2.

The TiO_2-F photocatalyst was prepared by wet impregnation of acidic fluoride solution.[38] 1 g of TiO_2 was dispersed in 50 mL of a solution containing 4% sodium fluoride (NaF 99%, Aldrich) and a suitable amount of nitric acid (HNO_3 99.5%, Fisher Scientific) to reach pH 3.2.[22] The powder was centrifuged and washed several times with diluted HNO_3 solutions (pH 3.2) and dried at 80 °C for 2 h.

Commercial Evonik P25® TiO_2 was used as reference photocatalyst. This sample is comprised of anatase (80%) and rutile (20%), presents a specific surface area of ca. 50 $m^2 \cdot g^{-1}$, and mean crystallite size of 30 nm. 1-Methylnaphtalene (95%) was purchased from Sigma-Aldrich and used as received without further purification.

Characterization Methods

The morphology and particle size of TiO_2 samples were determined by means of a JEOL JEM 1220 transmission electron microscope (TEM) operating at 120 kV. The samples were dispersed in water (0.1 wt%), deposited onto a thin Formvar film supported on a Cu grid, and dried in open air before TEM observation.

Thermogravimetric analyses (TGA) were performed with a Setaram SETSYS Evolution 12 thermoanalyzer coupled via a heated (ca. 150°C) fused silica capillary with Pfeiffer Omnistar quadrupole mass spectrometer (MS). TGA-MS studies were performed by heating the samples (40 mg in Pt-based open crucibles) from room temperature to 1100 °C at a constant rate of 10 °C·min^{-1} under nitrogen gas (50 $cm^3 \cdot min^{-1}$ STP).

Surface charge changes upon pH variation and the isoelectric point of the samples were determined by means of electrophoresis measurements by using a Zetasizer NanoZS (Malvern, UK). The zeta potential, ζ, was calculated from the electrophoretic mobility u_E using the Henry relationship under the Smoluchowski approximation for particles radius larger than the Debye length:

$$u_E = \frac{\varepsilon_0 \varepsilon \zeta}{\eta} \quad (1)$$

where η is the dynamic viscosity of water (η = 0.887 mPa·s at 25°C), ε_0 the vacuum permittivity, and ε the dielectric constant.

Diffuse reflectance UV-vis absorption spectra of the samples were recorded in the range 200–800 nm using a Shimadzu UV-2401PC spectrophotometer equipped with an integrating sphere. $BaSO_4$ standard was used as the reference.

X-ray photoelectron spectroscopy (XPS) was performed by using an Al Kα (1486.6 eV) source fitted to an Axis Ultra DLD spectrometer. High-resolution core levels analysis revealed chemical states attributable to C 1s, Ti 2p, F 1s and O 1s. The spectrum decomposition was carried out using a combination of Voigt functions with an overall full-width at half maximum (FWHM) of 1.6 eV.

Ultraviolet photoelectron spectroscopy (UPS) was performed by using the methodology developed by Cardenas et al.[34] UPS spectra were obtained by using a gas discharge UV lamp installed to an Axis Ultra DLD detector. UV lamp can deliver photons of 21.2 eV (He I) and 40.8 eV (He II). UPS measurements were collected using the He I resonance line as photon source, based on its high photoionization cross-section suitable for valence band analysis. Colloidal suspensions of TiO_2 and TiO_2-F powders dispersed in pentane (4 $g \cdot L^{-1}$) were deposited by drop-casting method on an Ag foil. The Ag surface was previously prepared using Ar^+ sputtering under ultra-high vacuum, allowing the Fermi level step and "4d" states to be easily observed by UPS. Ag UP spectrum was used for internal calibration to determine the absolute energy level positions of TiO_2 and TiO_2-F.

Photoelectrochemical measurements were performed in a 150 mL Pyrex reactor. 60 mg of the photocatalyst were added to 100 mL of a 0.1 M $NaNO_3$ solution and sonicated for 2 min. A platinum electrode and an Ag/AgCl were used as working and reference electrodes, respectively. The suspension was degassed for 30 min by bubbling N_2 and 25 mg methyl viologen (1,1'-dimethyl-4,4'-bipyridinium dichloride) were added. The pH value was adjusted using HNO_3 and NaOH solutions. During the potentiometric titration the suspension was irradiated by an UV lamp (Philips HPK 125 W), and the values of pH and potential (V) were measured by using a pH meter Thermo Orion 720A and a multimeter Metex3800, respectively.

Photoluminescence spectra were recorded by exciting the samples with a 10 mW CW laser model UF-F-355 (355 nm) from CNI laser, focused on a spot of 2 mm diameter. The

sample was placed on a Linkam stage THMS600 in which the temperature could be varied between 77 K and 873 K. The luminescence spectra were collected thanks to an optical fiber, and fed into a Jobin-Yvon TRIAX320 monochromator coupled to a Newton EMCCD from Andor. The resolution of the system was 2 nm for all of the performed measurements. Time-resolved photoluminescence was measured on the same apparatus. The excitation was performed by using an OPO laser from EKSPLA (NT230-50-SH) with a repetition rate of 50 Hz. The emission light was separated by a TRIAX320 monochromator and fed to a Peltier cooled Hamamatsu R943-02 photomultiplier (PMT). The PMT signal was then sent to a digital oscilloscope from Lecroy (model waverunner LT372). The signal was averaged over 4000 laser shots. Measurements were performed on two different time ranges in order to cover a large range of lifetimes.

The amount of fluorine in samples was determined by means of inductively coupled plasma optical emission spectrometry (ICP-OES, Axial ICP-OES Vista Agilent). Details on XRD, SEM and BET measurements are reported in Supporting Information.

Photocatalytic Degradation of 1-MN

Photocatalytic experiments were carried out in a double-jacketed cylindrical Pyrex batch photoreactor (diameter: 10 cm) containing 160 mL of a suspension of photocatalyst (1 $g \cdot L^{-1}$) in an aqueous solution of 1-MN (10 $mg \cdot L^{-1}$). The reaction temperature was adjusted at 298 K. The suspension was stirred at 500 rpm and illuminated by a PLL lamp UVA-cantered at 365 nm (8 $mW \cdot cm^{-2}$) placed horizontally below the photoreactor. Samples were collected at pre-specified time intervals and filtered through a Millipore PTFE 0.45 μm filter before liquid (HPLC) and gas (GC) chromatography analyses.

The evolution of the 1-MN concentration in the liquid phase was followed by injecting 50 μL into an HPLC system model 1290 Infinity (Agilent Technologies) equipped with a G4220B binary pump, a 1290 Infinity autosampler, a G4212B diode array detector (DAD), a G1321B fluorescence detector and a Polycyclic Aromatic Hydrocarbon (PAH) column (Agilent: 4.6×100 mm, 1.8 μm). Ultrapure water (solvent A) and acetonitrile (solvent B) were employed as the mobile phase with a flow rate of 1 $mL \cdot min^{-1}$ as follows: started with 60% A and 40% B, changed to 10% A and 90% B over 10 min, and finally, in 19 min take back to 60% A and 40% B for 1 min.

Data were collected by using the MassHunter software (Agilent). The concentration of 1-MN and degradation by-products in the reactor head space was detected by coupling the photoreactor online with an electronic-nose Heracles II (Alpha MOS France) equipped with a CombiPal autosampler. An electronic nose consists of a fast Gas Chromatography equipped with two columns working in parallel mode: a non-polar column (MXT5: 5% diphenyl, 95% methylpolysiloxane, 10 m length and 180 μm diameter) and a slightly polar column (MXT1701: 14% cyanopropylphenyl, 86% methylpolysiloxane, 10 m length and 180 μm diameter) connected to a dual Flame Ionization Detector. 5 mL of gas flow was collected in the head space cell (remote sampling site of the photoreactor) and injected in a cold Tenax® trap maintained at 15 °C. The gas desorbed from the trap at 240 °C was then flowed through the column by a H_2 carrier gas. The columns were maintained at 35 °C for 60 s, then brought to 260 °C at 3 °C·s^{-1} heating rate and kept at that temperature for 30 s before cooling down. Data were processed using AlphaSoft v14 software.

Results and Discussion

Structural and Morphological Characterization

X-ray diffraction patterns of both the TiO_2 and TiO_2-F photocatalysts (Figure S1 in Supporting Information) show the presence of anatase structure (JCPDS card: 21-1272) and the mean crystallite size of the nanoparticles, calculated by using the Debye-Scherrer equation, was about 11 nm. It is evident that fluorination does not produce structural changes in the bulk of the sample, the structural modification being merely near to the surface.

The morphology of TiO_2 and TiO_2-F samples was observed by TEM (Figure 1) and SEM (Figure S2 in Supporting Information) analyses. Surface fluorination did not affect the morphology. In fact, both the samples were made of aggregates of small faceted elementary nanoparticles with quite narrow size distribution, being the mean crystallite size of ca. 10 nm, according to the value calculated from the XRD patterns.

Nitrogen adsorption and desorption isotherms (Figure S3 in Supporting Information) of both TiO_2 and TiO_2-F samples showed the classical type IV adsorption isotherm, suggesting the presence of a mesoporous structure. At high relative pressure from 0.45 to 0.80, the isotherms exhibited hysteresis loops of H2 type indicating the existence of ink-bottle type pores with

narrow necks and wide bodies. The specific surface area calculated by using the Brunauer–Emmet–Teller (BET) equation was 103 $m^2 \cdot g^{-1}$ for both the samples. The pore size distribution, calculated by using the Barrett–Joyner–Halenda (BJH) equation was narrow and the average pore diameter was about 5 nm for both samples. Since the calculated pore size has the same order of magnitude of the elementary particles size, the retrieved porosity can be considered as deriving from interstices between the elementary nanoparticles. These results give evidence that surface fluorination does not induce modification of morphology and bulk structure.

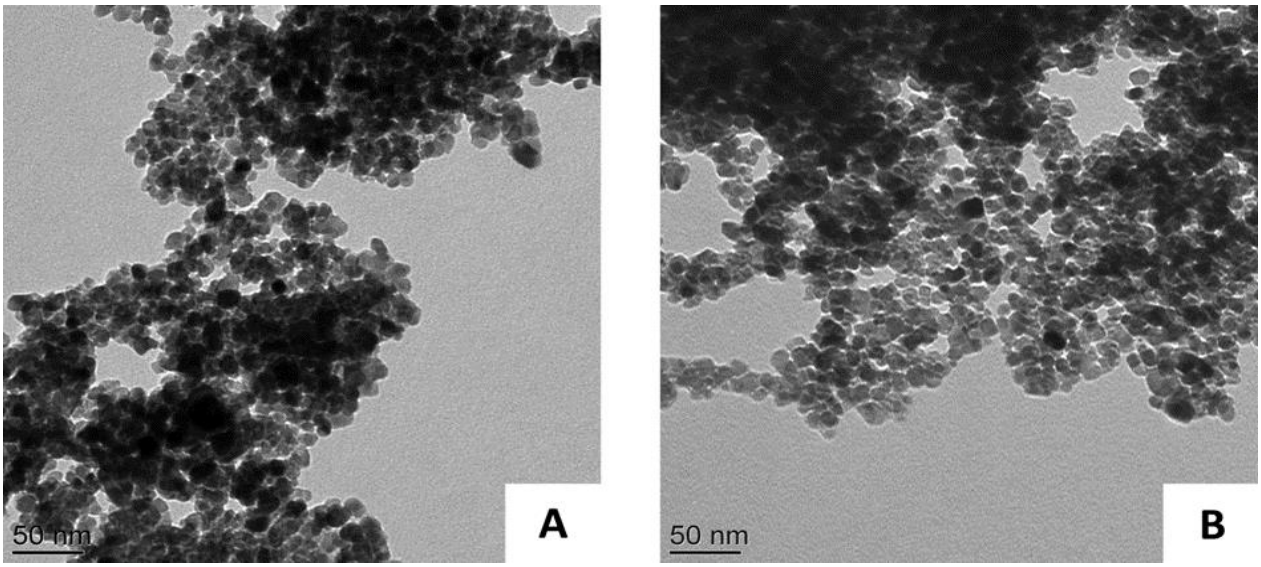

Fig 1. TEM micrographs of synthesized pristine TiO_2 (A) and TiO_2-F (B).

Surface Properties

Surface fluorination of TiO_2 can be considered as a simple ligand exchange between F^- ions and surface hydroxyl groups (Equation 2).[38]

$$Ti–OH + F^- \rightarrow Ti–F + OH^- \quad (2)$$

Equation 2 does not express a simple adsorption equilibrium because fluoride modification is stable upon washing during the preparation procedure and the reverse process, a nucleophilic substitution by hydroxide ions, requires high NaOH concentrations (ca. 1 M) and does not reach completion.[27] These observations indirectly indicate the formation of a chemical bond between titanium and fluorine.

The extent of TiO_2 fluorination was highly dependent on the pH of NaF solution. In fact, at acidic pH values (below the zero-point charge of TiO_2) surface protonation of TiO_2 results in formation of $Ti–OH_2^+$ species that activate nucleophilic substitution by fluoride ions. On the other hand, the acidic medium lowers the concentration of the nucleophilic F^- ions, as it shifts the equilibrium towards HF (p*K*a = 3.2). These opposite effects give rise to an optimum pH value maximizing the fluorination degree.[22] The surface density of fluorine groups on the TiO_2 surface was determined at various pH values by ICP-OES analysis. By taking into account the specific surface area of the TiO_2 sample (103 $m^2 \cdot g^{-1}$, Figure S3 in Supporting Information), results have been expressed in the form of fluorine surface density. In agreement with Minero et al.[22] the maximum fluorine surface density of 3 fluorinated surface sites per nm^2 was achieved at pH = 3.2 (Figure 2). This value corresponds to the substitution of ca. 50–60% of the total Ti–OH surface groups in the pristine TiO_2 (hydroxylation degree of 4.8–6.1 Ti–OH groups per nm^2).

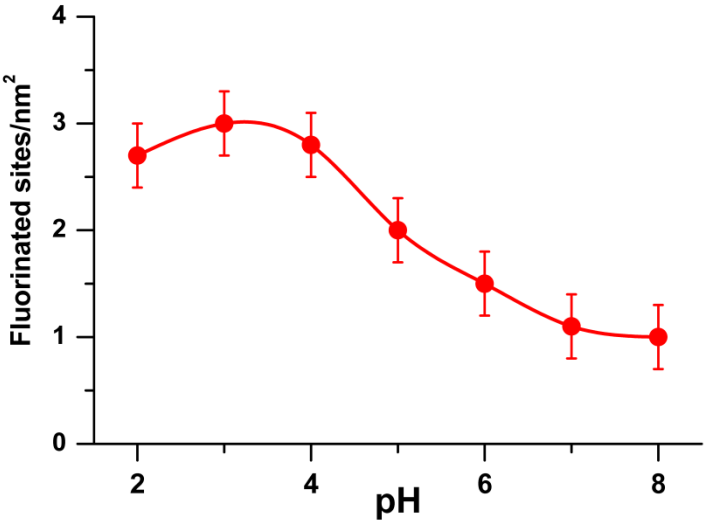

Fig 2. Amount of fluorinated sites obtained at different pH values of the starting NaF solution used for the modification. The experimental error has been estimated as 0.3 nm^{-2} in all experiments though no systematic repetitions have been performed.

TGA experiments of TiO_2 and TiO_2-F samples up to 900 °C are summarized in Figure 3. Heating up to 450 °C caused almost identical mass losses (ca. 4.5%) for both samples. In this range two mass loss stages are evident. The first, in the range 40–200 °C is related to

the removal of physically adsorbed water.[39,40] The slight deviation between TiO_2 and TiO_2-F samples in this range corresponds to a difference of surface hydration, being the TiO_2-F sample less hydrophilic than the pristine one. This is in agreement with the relevant literature.[32] The second step between 200 and 450 °C is attributed to the mass loss of water formed from condensation of surface hydroxyl groups.[39,40] Dehydration is almost complete at 500 °C. However, by considering the mass spectrometry analysis of the gases released in this temperature range, it is evident a slight mass drift up to 600 °C, showing further dehydration at higher temperatures. A third mass loss of about 3 wt% occurred only for the TiO_2-F sample in the range 450–600 °C. It was attributed to dehydrofluorination of the surface, as confirmed by the mass spectroscopy analysis of the HF-containing released gases between 450 and 600 °C. It was not possible to quantify the absolute amount of H_2O and HF released due to the unknown ionization efficiency of each compound. Moreover, being H_2O and HF simultaneously released, these data could not be used to confirm the fluorination extent retrieved by ICP-EOS analysis.

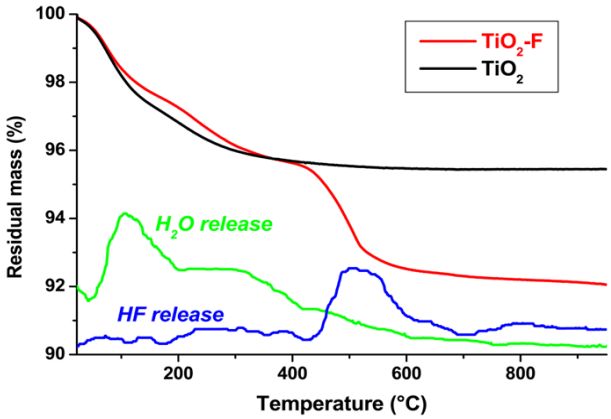

Fig 3. TGA thermographs of pristine TiO_2 (black line) and TiO_2-F (red line). The green and blue lines show the amount of released H_2O and HF, respectively, from TiO_2-F obtained by means of MS analysis. Notably, MS data are reported in arbitrary units, and do not refer to the vertical axis.

Zeta potential of both TiO_2 and TiO_2-F samples was measured as a function of pH (Figure 4) in order to determine the point of zero charge (*PZC*) of nanoparticles and to infer their stability in aqueous suspension. The *PZC* of pristine TiO_2 was 6.2 in agreement with values reported in literature.[41] On the other hand, the *PZC* of TiO_2-F was 4.0. The lower *PZC* of the fluorinated

sample indicates that the surface OH groups are protonated below pH = 4, i.e. the remaining Ti–OH surface groups are more acidic with respect to pristine TiO_2. This effect, already reported in the literature,[30] has been mainly ascribed to the enhanced Lewis acidity of Ti^{4+} sites when coordinating with very electronegative fluoride atoms. Moreover, it can be speculated that the lower concentration of OH groups on the surface of the fluorinated sample reduces the extent of hydrogen bonding between vicinal sites and reduces the range of stability of the protonated sites, which therefore behave as stronger Brønsted acids.

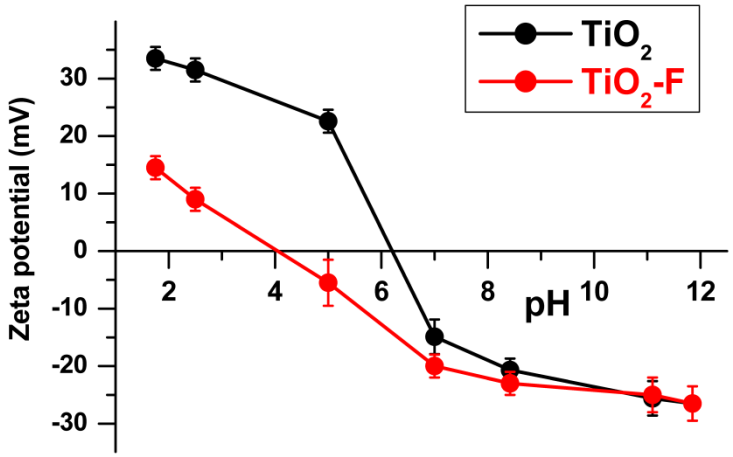

Fig 4. Zeta potential of TiO_2 and TiO_2-F particles in aqueous suspensions as a function of pH.

Electronic Properties

The electronic properties of pristine and surface fluorinated TiO_2 were investigated by the joint use of spectroscopies and photoelectrochemical techniques.

Diffuse reflectance spectroscopy in the UV-vis range provides information on the band gap of the material, i.e. on the excitation energy of electrons from the valence to the conduction band. Figure 5 shows that fluorine surface modification of TiO_2 led to a slight shift of absorbance towards the visible region compared to pristine TiO_2.

The absorbance has been calculated as a function of the reflectance (R'_∞) according to the Kubelka–Munk equation (Equation 3), where α and s are the absorption and the scattering coefficients, respectively

$$F(R'_\infty) = \frac{(1-R'_\infty)^2}{2R'_\infty} = \frac{\alpha}{s} \quad (3)$$

The inset of Figure 5 shows the plot of $[F(R'_\infty)\, h\nu]^{1/2}$ versus the incident photon energy ($h\nu$). The extrapolation of the linear part of the plot to the *x*–axis, defines the band gap energy of the samples considered as indirect band gap semiconductors. The values of the band gap retrieved through this procedure were 3.23 and 3.16 eV for TiO_2 and TiO_2-F, respectively. This difference is rather small but discloses slight changes in the electronic structure of the surface fluorinated sample with respect to the pristine one. However, a global shift keeping the band gap quasi-constant can take place; this does not prevent a redistribution of spectral weight concomitant with the formation of new electronic levels around of the pseudo Fermi level. It is worth to mention that no difference in terms of carbon or nitrogen impurities deriving from the preparation procedure could be detected by comparing FTIR (data not shown) and XPS analysis of pristine and fluorinated samples, so that the small changes in the UV-vis absorption should be attributed to the presence of fluorine. Though the absorption edge was only slightly affected by surface fluorination, Figure 5 shows a different optical behavior of the two powders. Similarly, Park and Choi[25,26] gave evidence of a higher light absorption (mainly in the UV region) when the surface of TiO_2 was fluorinated. This result has been related to the higher amount of adsorbed water in the case of TiO_2 with respect to TiO_2-F which enhances the amount of reflected photons and consequently reduces the absorbance with respect to the fluorinated sample. This hypothesis was also inferred in our case by taking into account the lower hydrophilicity of the TiO_2-F sample experimentally observed in the previous section by means of thermo-gravimetric analysis. On the other hand, insertion of fluoride into the crystal lattice of TiO_2 is sometimes reported to increase the light absorption and to cause a slight red shift in the band gap compared with pristine TiO_2.[42] Opposite evidences (no optical changes) have been reported by other authors,[33] so that this aspect needs to be further investigated. In our case, the mild preparation procedure makes fluorine insertion into the bulk of TiO_2 less probable; however, formation of Ti–F–Ti surface species cannot be in principle excluded.

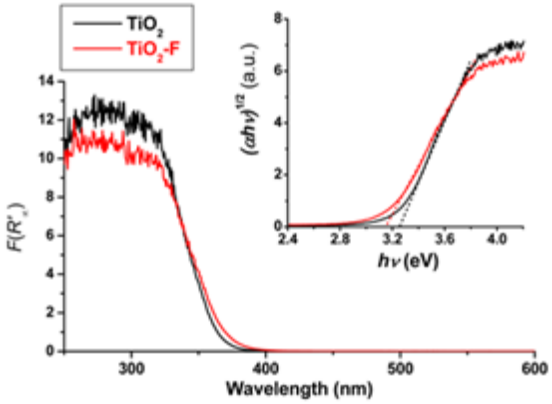

Fig 5. UV-vis diffuse reflectance spectra of synthesized pristine TiO_2 (black) and TiO_2-F (red). Plots of $(\alpha h\nu)^{1/2}$ versus $h\nu$ (inset).

To address this issue, XPS and UPS analysis were performed. Insertion of fluorine into the TiO_2 lattice would result in formation of Ti^{3+} centers, which localize the extra electron needed for charge compensation. The full XPS spectra of TiO_2 and TiO_2-F samples are shown in the Supporting Information Section (Figure S4 in Supporting Information). Figure 6 shows the Ti 2p and F 1s core level signals related to pristine TiO_2, TiO_2-F, and a commercial TiF_4 sample purchased from Sigma-Aldrich. In some cases, samples have been sputtered under Ar^+ etching treatment.

The different core levels of Ti in TiO_2 and TiO_2-F are shown in Figure 6a. The spin orbit states of Ti $2p_{3/2}$ at 458.2 eV and Ti $2p_{1/2}$ at 464.0 eV can be attributed to Ti^{4+} species and they are present both in the TiO_2 and TiO_2-F sample. However, no trace of Ti^{3+} species coming from fluorine insertion is visible at 457.0 eV in the Ti 2p level of the spectrum of TiO_2-F, confirming that, if present, Ti–F–Ti groups on the TiO_2 surface are below the detection limit of XPS. Similarly, no Ti(II) species, which would produce a signal at 455.2 eV, could be seen.

The analysis of the F 1s state for TiO_2-F surface (Figure 6b, blue line) revealed a single contribution at 684.3 eV which, as expected, is absent in the spectrum of pristine TiO_2 (data not shown). The spectrum of TiF_4 taken as reference (Figure 6c, blue line) showed the same state at 684.3 eV, confirming the presence of Ti–F bonds on the surface of TiO_2-F sample.

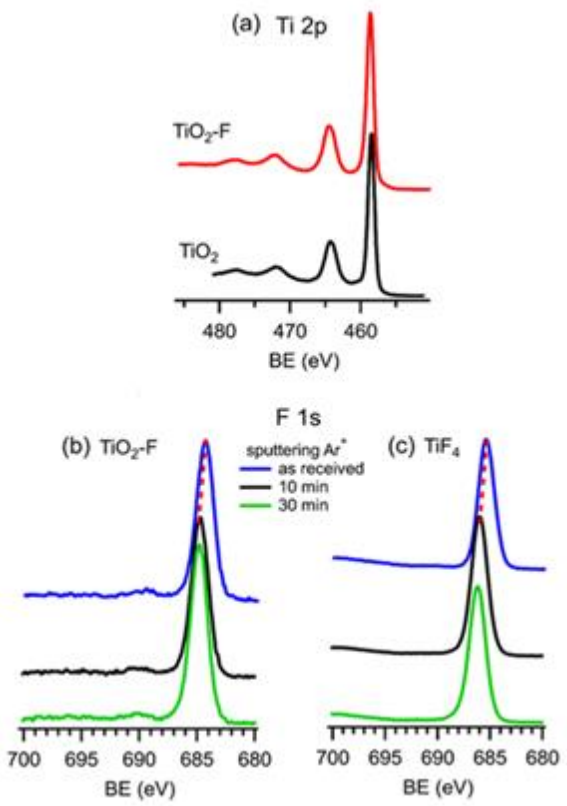

Fig 6. (a) Ti 2p core levels in TiO_2 (black line) and TiO_2-F (red line) samples. F 1s core levels in TiO_2-F (b) and TiF_4 (c) samples before (blue line), after Ar^+ sputtering for 10 min (black line), and for 30 min (green line).

However, the binding energy of the Ti–F bond is shifted by few hundreds meV with respect to literature values,[43,44] indicating a contamination by atmospheric oxygen-containing species (water, CO_2, organics) interacting with the fluorinated surface of both TiO_2-F and TiF_4. This could induce a variation of the chemical environment at the surface and influence the binding energy of the Ti–F bond, possibly leading to misinterpretation due to the spectral resolution and differential charge effects on the surface. In order to check against this hypothesis, both the TiF_4 and TiO_2-F samples have been treated with Ar^+ sputtering under ultra-high vacuum at 1 keV for 10 and 30 min. Ar^+ etching removes from the surface air-borne molecules, leaving the sole F bound to Ti atoms. As a consequence of Ar^+ sputtering, the signals of the Ti–F bond of both TiF_4 and TiO_2-F shifted towards higher binding energies (of ca. 0.4 eV for TiO_2-F and 0.6 eV for TiF_4) in agreement with literature data. Ti–F bonds were kept in both cases even after prolonged

Ar^+ etching (30 min, green line Figures 6b and c) thus providing clear demonstration that stable covalent Ti–F bonds have been formed at the surface of TiO_2-F. Notably, the F 1s peak at 684.3 eV, observed in the non-sputtered sample, has been previously assigned to combination of non-resolved peaks of bound fluorine atoms and adsorbed fluoride anions.[45] However, according to our results, the presence of residual adsorbed fluoride anions was discarded because of the similar behavior observed with pure TiF_4 that does not contain fluoride anions.

Finally, even if fluorine insertion into the bulk of anatase can be excluded because of the absence of the characteristic F 1s peak at 688.3 eV,[42] a weak F 1s peak at ca. 690 eV might correspond to very small amounts of bridging fluorine (Ti–F–Ti) at the surface of TiO_2. Such signal has been observed in case of bulk fluorination, e.g. for bulk F-doped TiO_2 samples prepared by sol-gel synthesis by using NH_4F as a precursor.[42] The trace amount of Ti–F–Ti groups which could be detected by XPS analysis, justifies that only slight changes were observed by the poorly sensitive UV-vis diffuse reflectance spectroscopy technique, and the contradictory results often reported in literature on the optical properties of surface fluorinated TiO_2.

In order to gain further evidences on the possible electronic interactions between surface fluorine species and the semiconductor structure of TiO_2, UPS analysis was performed by using the particular expertise developed by Cardenas et al.[34] This technique affords spectra of electronic states related to the valence band against the vacuum level with spectral resolution (0.15 eV) more than five times higher than XPS (0.6 eV). Indeed, the photoionization cross-section of titanium is ca. 10,000 times higher for UV excitation (21.2 eV) than for X-rays (1486.6 eV).[45] Moreover, as a lower photoelectron energy range is probed, only electrons coming from the extreme surface of the material can be excited and the technique results very surface sensitive (the analyzed depth is ca. 1 nm). For these reasons, UPS is a powerful technique for the purpose of the present investigation.

Both TiO_2 and TiO_2-F samples produce a broad signal between 13 and 2 eV (Figure 7a). TiO_2 spectrum exhibits three bands. The broad band at ca. 6 eV and the one at 8.5 eV correspond to hybridization between Ti and nonbonding and bonding O 2p orbitals.[46] The small band at around 11 eV can be attributed to surface OH groups.[47] The band assignment for TiO_2-F sample is much more complex. The observed differences between

TiO_2 and TiO_2-F can be attributed to the contribution of F 2p orbitals.[48] Notably, signal related to trivalent Ti^{3+} 3d species was expected at around –1 eV from E_F as it has been observed with reduced TiO_2 and bulk-doped TiO_2;[49–53] it has not been observed in both present samples, confirming the XPS results. Notably, the band at 11 eV is negligible in the TiO_2-F sample further confirming the above mentioned substitution of surface OH groups with covalently bound fluorine atoms. By magnifying the spectrum in the region of the edge of the valence band (Figure 7b), it is evident that photoelectrons can be excited at lower energy in the case of TiO_2-F with respect to pristine TiO_2. This important upward shift of the valence band by ca. 1.3 eV indicates the presence of intermediate intra band gap energy levels in the fluorinated sample. Such states, appearing as the presence of a tail ranging between 1.3 and 2.6 eV in Figure 7, are localized close to the valence band. In order to estimate the position of these intermediate energy states with respect to the conduction band, the absolute position of the conduction band edge was determined.

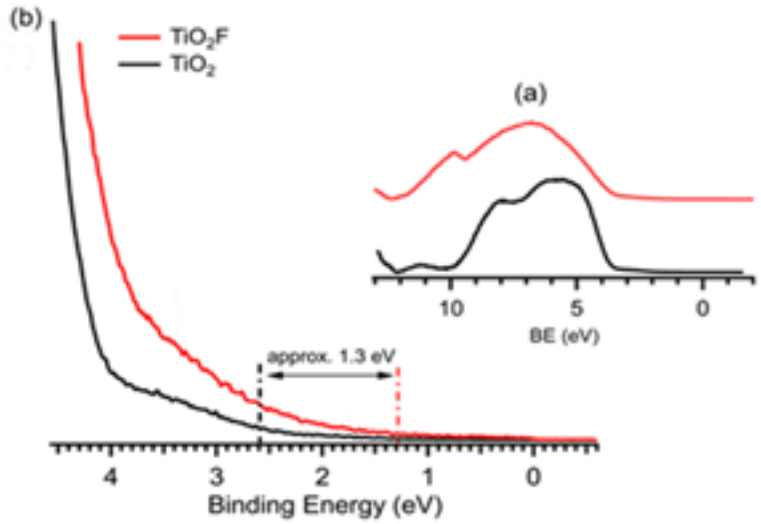

Fig 7. UPS spectra of TiO_2 and TiO_2-F. Binding energy is expressed with respect to the vacuum energy level. (a): Wide UPS scan between 13 and –2 eV. (b): Local spectral zone between 4.5 and –0.6 eV.

Photoelectrochemical measurements allow the determination of the chemical potential of electrons. The potential of the photogenerated electrons in TiO_2-F should be cathodically

shifted with respect to bare TiO_2 if these states were located close to the conduction band, while it should be virtually the same if they were located close to the valence band. The measurement is based on the assumption, valid for n-type semiconductors such as TiO_2 that the shift between the quasi Fermi level of electrons and the conduction band edge is virtually negligible.

The values of the flat band potential (E_{FB}) of the TiO_2 and TiO_2-F samples were determined using the slurry method proposed by Roy et al.,[54] by measuring the variation of the photovoltage with respect to the pH of suspensions of powders in the presence of an electron acceptor (methyl viologen dichloride). The pH value at the inflection point (pH_0) of the obtained sigmoidal curves shown in Figure 8 allows the calculation of the flat band potential at pH 7 according to Equation 4

$$E_{FB}\,(pH=7) = E^{0}_{MV^{2+}/MV^{+\bullet}} + 0.059\,(pH_0 - 7) \qquad (4)$$

where $E^{0}_{MV^{2+}/MV^{+\bullet}}$ is the standard potential of the redox couple $MV^{2+}/MV^{+\bullet}$ equal to −0.445 V vs (NHE).[55]

The values obtained were −0.53 ± 0.4 V vs (NHE) for TiO_2-F and −0.56 ± 0.4 V vs (NHE) for pristine TiO_2. Being the reproducibility of ± 0.04 V for the determination of flat band potential, no remarkable differences in the absolute potential of the photogenerated electrons can be observed between the two samples, so that it can be concluded that the intermediate energy states disclosed by UPS analysis are located close to the valence band.

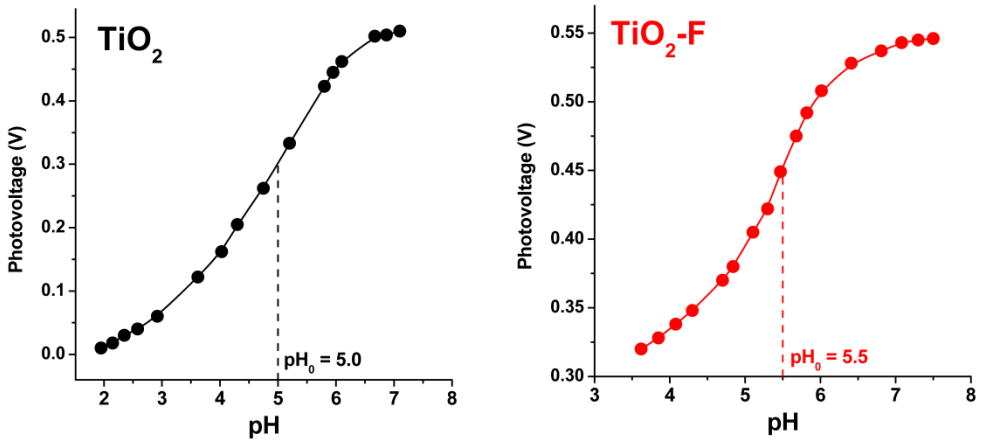

Fig 8. Effect of pH on the photovoltage developed by irradiation of TiO_2 (left) and TiO_2-F (right). Each experiment was repeated 3 times and reproducibility was better than ± 20 mV.

The results obtained from UPS, DRS and photoelectrochemical measurements allow schematically summarizing the electronic structure of the samples as shown in Figure 9. It is worth to keep in mind that the values reported in Figure 9 have been experimentally retrieved. The band gap values were obtained by DRS analysis. Photoelectrochemical measurements allowed experimentally determining the conduction band edge, by assuming negligible the difference between the Fermi level of the n-type semiconductor and its conduction band. Adding the conduction band edge potential to the band gap affords the valence band edge, which turns being the same as the experimental value measured by means of UPS. Moreover, UPS analysis (Figure 7) coupled with photovoltage measurements (Figure 8) gives evidence that the intermediate energy states are spread within 1.3 eV above the valence band of TiO_2-F.

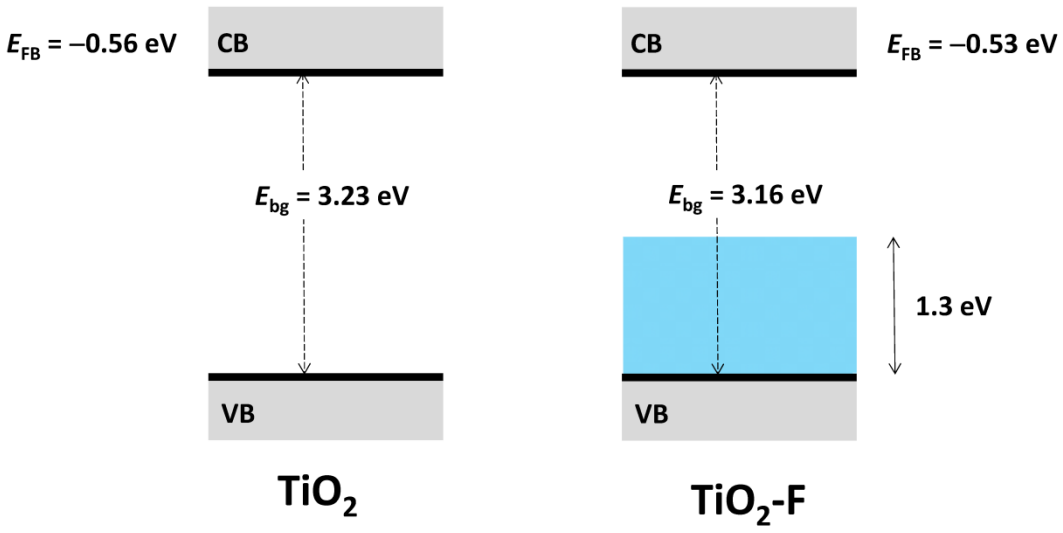

Fig 9. Schematic diagram representing the electronic structure of TiO_2 and TiO_2-F. The light blue part shows the position of the intermediate energy levels inside the band gap.

To the best of our knowledge, the presence of these intermediate energy states has been here experimentally observed for the first time. In fact, even if considered as a surface analysis technique, XPS was not able to reveal fluorination-induced changes of electronic states because this technique probes quite a large depth of several atomic layers, while fluorine modification is hereby confined only at the surface. Instead, UPS provides an analysis of energy states at the very top surface layers of the material, thus highlighting the influence of surface fluorine atoms. Such a large effect on the electronic structure of the semiconductor (1.3 eV) induced by a simple surface fluorination may appear surprising. The pertinent literature reporting experimental results is often difficult to be compared, due to the various preparation protocols, morphologies, and structures of TiO_2, which consequently influence the photocatalytic activity in a different way. Only recently, a rational experimental approach has been proposed[32,56] to determine the influence of surface and bulk fluorination on photocatalytic activity.

Instead, theoretical works are mainly focused on the bulk fluorination of TiO_2,[33] and those approaching the influence of surface fluorination provide often contrasting results. In particular, Kus et al.[57] performed DFT calculations on anatase {001} surfaces with different terminations. By keeping the same bulk structure, the HF-covered surface caused a downward (anodic) shift of the bands of 1.4 eV with respect to the clean surface. On the other hand, DFT calculations by Guo et al.[58] demonstrated that the fluorinated surface induced an upward (cathodic) valence band shift of 1.11 eV with respect to the pristine rutile {110} surface. Moreover, DFT calculations by Lamiel-Garcia et al.[59] demonstrated that fluorination of anatase TiO_2 {101} induced intra band gap energy states localized at ca. 1.3 eV above the valence band (towards the negative potentials). Instead, for TiO_2 {001} surfaces, fluorination produced a significant reduction of the band gap by introducing additional energy states below and above the conduction and valence band, respectively. Authors also report that the extent of these changes decreases by decreasing the fluorination degree of the surface, but are fully visible already for coverages of ca. 30%. All of these reports, even if controversial with regard to the nature of the energy states, confirm that surface fluorination can induce remarkable changes of the order of ca. 1 eV, supporting the experimental results hereby reported.

The classical theory of semiconductor junctions by Tamm and Shockley provides support showing how slight modifications of the surface cause large effects on bulk electronic properties. The influence of electronic states at the surface of semiconductors is first the formation of well-defined 'intrinsic' surface electronic states within the band gap.[60,61] The second consequence is bending the VB and CB. As the Fermi levels of bulk and surface electrons are the same, electrons filling surface states from the subsurface region leave there a depletion region that causes upward band bending of an n-doped semiconductor. Band bending coming from the electrostatic effect of the space charge is the same for VB and CB, so it does not change the band gap energy. Such surface phenomena are operating at all semiconductor–vacuum interfaces. Band bending can extend over a large part of the band gap of bulk materials.[61] It is weak for small semiconductor particles because of the confinement of the electrical double layer in the space charge region.[62] So, surface states set bulk properties by 'Fermi level pinning'. Chemical modification of the surface strongly affects bulk electronic properties and photocatalytic activity in that way.

The intermediate energy levels result in different photoluminescence emission behavior of TiO_2-F with respect to the pristine TiO_2 material. Emission spectra of TiO_2 and TiO_2-F have been recorded at different temperatures ranging from –190 °C to 20 °C. Figure 10 shows them at the limit temperatures considered. The spectra recorded at intermediate temperatures are reported in Figure S5 in Supporting Information.

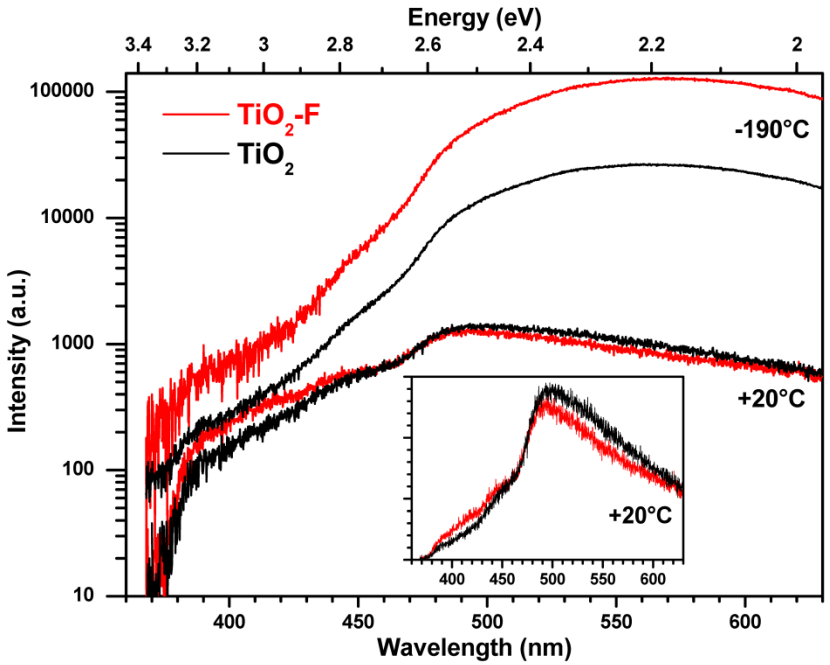

Fig 10. Photoluminescence spectra of pristine TiO_2 (black lines) and TiO_2-F (red lines) at +20 °C and –190 °C. The 355 nm excitation wavelength has been cut off with a long-pass filter at 380 nm. The inset shows the photoluminescence spectra of TiO_2 (red line) and TiO_2-F (black line) recorded at +20 °C in linear scale.

The differences between the two samples obviously appeared at low temperatures, while the emission behavior is virtually the same at room temperature. For both the samples emission was weak between 380 and 400 nm while it increased at longer wavelength. Therefore, emission from free excitons is less probable, as expected for an indirect bandgap semiconductor such as TiO_2, while most emitted photons have longer wavelengths. Such emission has been ascribed to the presence of empty levels of Ti^{3+} within the band gap, slightly below the CB.[63,64] The higher emission observed at low temperature for the TiO_2-F sample with respect to bare TiO_2 confirms the existence of intermediate energy levels disclosed by UPS spectroscopy. This effect is visible at low temperature because vibration quenching occurring at low temperature decreases non-radiative de-excitation, thus revealing the stronger emission of TiO_2-F at longer wavelengths. Light emission by radiative decay of the excited states was measured by time resolved photoluminescence spectroscopy, which gave information on the life-time

of the excited species. This information is of high relevance since efficient photocatalytic activity generally requires long living photoexcited states. Measurements were performed at 500 nm and –190 °C (Figure 11).

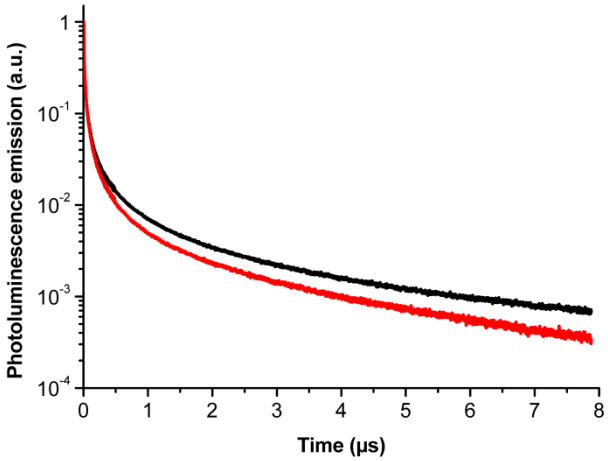

Fig 11. Time-resolved photoluminescence of pristine TiO_2 (black line) and TiO_2-F (red line) at 500 nm and 77 K.

The emission decay of the excited states is faster for TiO_2-F than TiO_2. The mean relaxation time, $\bar{\tau}$ estimated as the time when half the energy has been emitted through Equation 5 was 0.24 ± 0.02 μs for TiO_2 and 0.13 ± 0.02 μs for TiO_2-F.

$$\int_0^{\bar{\tau}} I(t)\,dt = \frac{1}{2}\int_0^{\infty} I(t)\,dt \qquad (5)$$

Photoluminescence decays were not purely exponential. This can be ascribed to a distribution of several types of excited states emitting light at the same wavelength, or to a distribution of non-radiative de-excitation paths (recombination channels) from the same state. In order to discriminate these two cases, the non-exponential decay was modelled using a classical Kohlrausch stretched exponential[65] (Figure S6 in Supporting Information) according to Equation 6

$$I(t) = I(0)\exp\left(-\left(\frac{t-t_0}{\tau}\right)^{\beta}\right) \qquad (6)$$

where τ is a time constant, β describes the width of the distribution ($0 \leq \beta \leq 1$), and t_0 is the start time hidden by the excitation pulse. The β exponent characterizes the width of the distribution and have nearly the same value for TiO_2 and TiO_2-F, i.e. $\beta = 0.080 \pm 0.002$. A distribution of radiative excited states would be characterized by quite a large value of β ($0.5 < \beta < 1$).[66–69] The very low value of β reveals a broad distribution of non-radiative deexcitation paths coming from an increased density of non-radiative centers.

Non-radiative de-excitation is attenuated at low temperature (77 K), so that radiative transitions were detected with higher sensitivity. Since the shorter lifetime observed for TiO_2-F was ascribed to a faster non-radiative decay coming from a larger density of recombination paths, the luminescence quantum yield should be lower for TiO_2-F. Therefore, the origin of higher luminescence observed for TiO_2-F is a larger density of defects emitting light. As a whole, fluorination causes both increased densities of defects emitting light and non-radiative centers. The presence of intermediate energy states within the band gap of TiO_2-F causes faster de-excitation with prevalent non-radiative character compared to bare TiO_2.

Photocatalytic Activity

Figure 12 shows the kinetics of 1-MN photodegradation in the presence of pristine TiO_2, TiO_2-F and commercial P25 TiO_2 (Evonik) under UV light. P25 TiO_2 was used as a reference in order to compare the photocatalytic activity of TiO_2 and TiO_2-F samples with a commercial benchmark. The suspension containing 1-MN was maintained in the dark under stirring during 180 min before irradiation. 1-MN adsorption reached equilibrium after ca. 30 min for all samples. Notably, the initial concentration of 1-MN was below its solubility limit in water. Tests in biphasic conditions are ongoing and will be subsequently reported. Under UV light irradiation degradation of 1-MN started. Figure 12 reports the 1-MN concentration decrease in the liquid phase and in the head-space gas, demonstrating the effective degradation of the substrate. The degradation of the 1-MN was faster in the presence of TiO_2-F than both pristine TiO_2 and P25.

The present results show that fluorination of TiO_2 results in enhanced 1-MN degradation with respect to both pristine TiO_2 sample and to the benchmark TiO_2 P25.

The activity of a photocatalyst is the result of the complex interplay between various factors. In the present case both pristine and surface fluorinated TiO_2 possess similar morphological and structural properties, so that the higher photocatalytic efficiency of TiO_2-F can be associated with the surface and opto-electronic features.

As far as the surface features are concerned, it has been shown from TGA analysis that the surface of the fluorinated sample is slightly less hydrophilic that the pristine TiO_2. This would favor the adsorption of 1-MN, as it results from the slightly higher amount of 1-MN adsorbed under dark conditions (Figure 12a). Even though the surface features dramatically change under irradiation, the proximity of 1-MN molecules to the surface of TiO_2 could be beneficial for the photocatalytic degradation both if it occurs directly through photogenerated holes or indirectly through $OH^{\bullet}$ radical mediated oxidation. It must be mentioned, that surface fluorinated TiO_2 produces higher amount of $OH^{\bullet}$ radicals with respect to pristine TiO_2 because the holes in the valence band are not able to oxidize surface fluorine groups because the oxidation potential of the $F^{\bullet}/F^{-}$ couple is too high (3.6 V). Therefore, hole-induced oxidation of water producing $OH^{\bullet}$ radicals is favored.

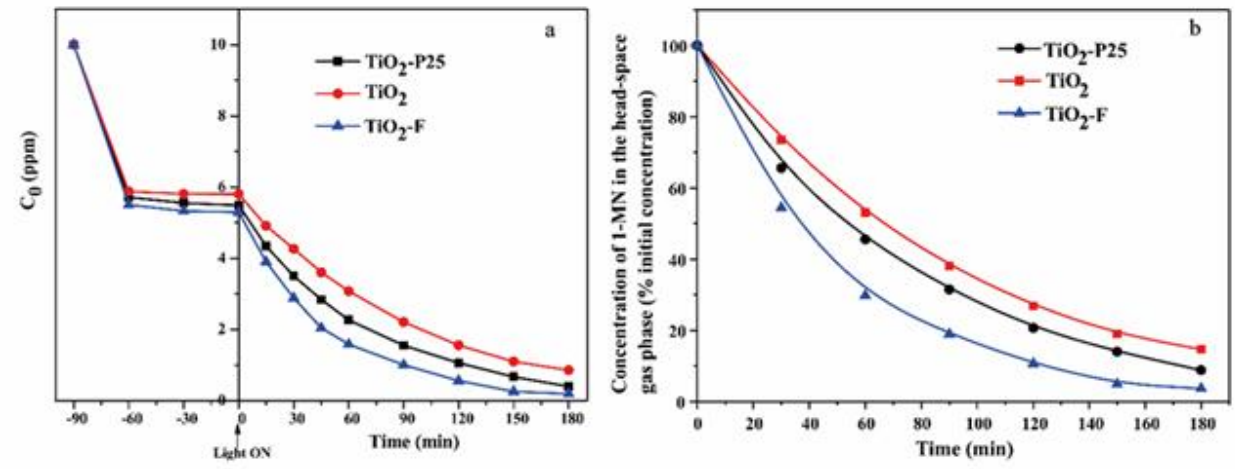

Fig 12. Degradation of 1-MN over pristine TiO_2, TiO_2-F and P25 under UV irradiation. Concentration of 1-MN in liquid phase (a) and in the head-space gas phase (b) was analyzed by HPLC and by electronic nose GC analysis, respectively.

The strong interaction of 1-MN with the TiO_2-F surface can be explained by comparing the standard adsorption free energy with the thermal energy. After equilibrium during dark

adsorption, the 1-MN concentration residual in solution was C_{res} = 5.5 ppm (38.7 µmol·L^{-1}), out of the initial C_{tot} = 10 ppm (70.3 µmol·L^{-1}). Therefore it is possible to calculate the surface concentration of adsorbed 1-MN, Γ = 0.307 µmol·m^{-2}, according to Equation 7.

$$\Gamma = \frac{(C_{tot} - C_{res})V}{M\, A_{sp}} \quad (7)$$

where M/V = 1 g·L^{-1} is the dispersed amount of catalyst and A_{sp} = 103 m^2·g^{-1} is its specific area. The equilibrium constant for 1-MN adsorption was estimated assuming a Langmuir-type adsorption isotherm (Equation 8).

$$K = \frac{\Gamma}{(\Gamma_{max} - \Gamma)\, C_{res}} \quad (8)$$

The surface concentration at full monolayer coverage was 2.8 µmol·m^{-2}, as calculated from the molecular area of 1-MN adsorbed flat to a surface (60 Å^2).[70] By using concentrations expressed in mol·L^{-1}, the equilibrium constant obtained through Equation 8 is K = 3200 (Log$K$ = 3.5), which corresponds to a standard free energy of adsorption much larger than thermal energy: $\Delta_{ads}G^0$ = –20 kJ·mol^{-1} (~8 RT).

Finally, surface fluorination might enhance photocatalytic activity because of the better dispersibility of the photocatalyst in aqueous medium,[71] leading to a better contact with 1-MN molecules in the medium. The observed shift of the point of zero charge (PZC) upon fluorination from 6.2 to 4.0 makes TiO_2-F particles negatively charged at neutral pH (between 6 and 7), whereas TiO_2 particles are quasi-neutral (PZC = 6.2). Electrostatic repulsions between TiO_2-F particles provide a better dispersion and efficiently stabilize the dispersion during the photocatalytic process.

As far as the electronic properties are concerned, we hereby demonstrated the existence of localized intra band gap energy levels within ca. 1.3 eV above the valence band for the TiO_2-F sample. The resulting slightly different optical features of the fluorinated sample with respect to the pristine TiO_2 can be beneficial to the photocatalytic activity. Thus, excitation can occur at lower energy of the incident radiation and these centers can behave as active sites promoting photocatalytic activity. The higher defect density observed for the TiO_2-F caused higher emission and faster charge recombination compared to bare TiO_2. De-excitation occurs through both radiative and non-radiative pathways. So it can be inferred that the higher density of electronic defects may be beneficial to the

photocatalytic activity, regardless the slightly shorter life time of the electron-hole pairs. The presence of intermediate energy states can also explain the reported enhanced generation of singlet oxygen in the presence of TiO_2-F.[72,73] Energy emission from these states can induce excitation of oxygen from the triplet to the singlet state that would hardly occur in bare TiO_2 due to the mismatch between the band gap energy and the oxygen excitation energy.

Conclusions

Surface fluorinated TiO_2 has been extensively investigated as a robust and promising photocatalyst for the photocatalytic degradation of polycyclic aromatic hydrocarbon 1-methylnaphtalene. Evidence has been given that the morphology and the structural features of TiO_2 do not change upon fluorination. On the other hand, significant modifications have been induced as far as the surface and opto-electronic features are concerned. In particular, it has been shown that fluorination reduces the hydrophilic character of TiO_2 and shifts the point of zero charge of TiO_2 towards lower pH values. Moreover, it has been highlighted for the first time that surface fluorination induces intra band gap energy states within 1.3 eV above the valence band. Combination of UPS and photoelectrochemical measurements specified the position of such energy levels close to the valence band. These features have been related with the photocatalytic activity of the fluorinated TiO_2 sample for the degradation of 1-methylnaphtalene, which is ca. twice higher with respect to both the pristine TiO_2 sample and to the commercial Evonik P25.

Supporting Information

X-ray diffraction, SEM, BET, XPS and photoluminescence measurements that are not included in the main text.

Acknowledgment

NF acknowledges a fellowship for travelling from the Tunisian Ministry of Higher Education and Scientific Research as a support to this international collaborative project.

Conflicts of interest

There is no conflict of interest to declare.

References

(1) Camera-Roda, G.; Loddo, V.; Palmisano, L.; Parrino, F. Photocatalytic Ozonation for a Sustainable Aquaculture: A Long-Term Test in a Seawater Aquarium. *Appl. Catal. B: Environ.* **2019**, *253*, 69–76.

(2) Hoffmann, M. R.; Martin, S. T.; Choi, W.; Bahnemann, D. W. Environmental Applications of Semiconductor Photocatalysis. *Chem. Rev.* **1995**, *95*, 69–96.

(3) Mills, A.; Le Hunte, S. An Overview of Semiconductor Photocatalysis. *J. Photochem. Photobiol. A: Chem.* **1997**, *108*, 1–35.

(4) Fujishima, A.; Rao, T. R.; Tryk, D. A.; Titanium Dioxide Photocatalysis. *J. Photochem. Photobiol. C: Photochem. Rev.* **2000**, *1*, 1–21.

(5) Parrino, F.; Camera-Roda, G.; Loddo, V.; Palmisano, L. Green Synthesis of Bromine by TiO_2 Heterogeneous Photocatalysis and/or Ozone: A Kinetic Study. *J. Catal.* **2018**, *366*, 167–175.

(6) Abd-Elaal, A.; Parrino, F.; Ciriminna, R.; Loddo, V.; Palmisano, L.; Pagliaro, M. Alcohol-Selective Oxidation in Water under Mild Conditions via a Novel Approach to Hybrid Composite Photocatalysts. *Chemistry Open* **2015**, *4*, 779–785.

(7) Parrino, F.; Di Paola, A.; Loddo, V.; Pibiri, I.; Bellardita, M.; Palmisano, L. Photochemical and Photocatalytic Isomerization of *trans*-Caffeic Acid and Cyclization of *cis*-Caffeic Acid to Esculetin. *Appl. Catal. B: Environ.* **2016**, *182*, 347–355.

(8) Paz, Y.; Luo, Z.; Rabenberg, L.; Heller, A. Photooxidative Self-Cleaning Transparent Titanium Dioxide Films on Glass. *J. Mater. Res.* **1995**, *10*, 2842–2848.

(9) Fretwell, R.; Douglas, P. An Active, Robust and Transparent Nanocrystalline Anatase TiO_2 Thin Film — Preparation, Characterisation and the Kinetics of Photodegradation of Model Pollutants. *J. Photochem. Photobiol. A: Chem.* **2001**, *143*, 229–240.

(10) Roméas, V.; Pichat, P.; Guillard, C.; Chopin, T.; Lehaut, C. Degradation of Palmitic (Hexadecanoic) Acid Deposited on TiO_2-Coated Self-Cleaning Glass: Kinetics of Disappearance, Intermediate Products and Degradation Pathways. *New J. Chem.* **1999**, *23*, 365–373.

(11) Roméas, V.; Pichat, P.; Guillard, C.; Chopin, T.; Lehaut, C. Self-Cleaning Properties of TiO_2-Coated Glass: Degradation, under Simulated Solar Light, of Palmitic (Hexadecanoic) Acid and Fluoranthene Layers Deposited on the Glass Surface. *J. Phys. IV France* **1999**, *9(Pr3)*, 247–252.

(12) Hegazy, A.; Kinadjian, N.; Sadeghimakki, B.; Sivoththaman, S.; Allam, N. K.; Prouzet, E. TiO_2 Nanoparticles Optimized for Photoanodes Tested in Large Area

Dye-Sensitized Solar Cells (DSSC). *Solar Energy Materials and Solar Cells* **2016**, *153*, 108–116.

(13) Zhao, T.; Luo, W.; Deng, Y.; Luo, Y.; Xu, P.; Liu, Y.; Wang, L.; Ren, Y.; Jiang, W. Monodisperse Mesoporous TiO_2 Microspheres for Dye Sensitized Solar Cells. *Nano Energy* **2016**, *26*, 16–25.

(14) Yamaguchi, S.; Kobayashi, H.; Narita, T.; Kanehira, K.; Sonezaki, S.; Kudo, N.; Kubota, Y.; Terasaka, S.; Houkin, K. Sonodynamic Therapy using Water-Dispersed TiO_2-Polyethylene Glycol Compound on Glioma Cells: Comparison of Cytotoxic Mechanism with Photodynamic Therapy. *Ultrason. Sonochem.* **2011**, *18*, 1197–1204.

(15) Lopez, T.; Ortiz, E.; Alvarez, M.; Navarrete, J.; Odriozola, J. A.; Martinez-Ortega, F.; Páez-Mozo, E. A.; Escobar, P.; Espinoza, K. A.; Rivero, I. A. Study of the Stabilization of Zinc Phthalocyanine in Sol-Gel TiO_2 for Photodynamic Therapy Applications. *Nanomed. Nanotechnol. Biol. Med.* **2010**, *6*, 777–785.

(16) Ibhadon, A. O.; Fitzpatrick, P. Heterogeneous Photocatalysis: Recent Advances and Applications. *Catalysts* **2013**, *3*, 189–218.

(17) Parrino, F.; De Pasquale, C.; Palmisano, L. Influence of Surface-Related Phenomena on Mechanism, Selectivity, and Conversion of TiO_2-Induced Photocatalytic Reactions. *Chem. Sus. Chem.* **2019**, *12*, 589–602.

(18) Cataldo, S.; Iannì, A.; Loddo, V.; Mirenda, E.; Palmisano, L.; Parrino, F.; Piazzese, D. Combination of Advanced Oxidation Processes and Active Carbons Adsorption for the Treatment of Simulated Saline Wastewater. *Sep. Purif. Technol.* **2016**, *171*, 101–111.

(19) Toledano-Garcia, D.; Ozer, L. Y.; Parrino, F.; Ahmed, M.; Brudecki, G. P.; Hasan, S. W.; Palmisano, G. Photocatalytic Ozonation under Visible Light for the Remediation of Water Effluents and Its Integration with an Electro-Membrane Bioreactor. *Chemosphere* **2018**, *209*, 534–541.

(20) Parrino, F.; Corsino, S. F.; Bellardita, M.; Loddo, V.; Palmisano, L.; Torregrossa, M.; Viviania, G. Sequential Biological and Photocatalysis Based Treatments Forshipboard Slop Purification: A Pilot Plant Investigation. *Process Saf. Environ. Prot.* **2019**, *125*, 288–296.

(21) Fessi, N.; Nsib, M. F.; Chevalier, Y.; Guillard, C.; Dappozze, F.; Houas, A.; Palmisano, L.; Parrino, F. Photocatalytic Degradation Enhancement in Pickering Emulsions Stabilized by Solid Particles of Bare TiO_2. *Langmuir* **2019**, *35*, 2129−2136.

(22) Minero, C.; Mariella, G.; Maurino, V.; Pelizzetti, E. Photocatalytic Transformation of Organic Compounds in the Presence of Inorganic Anions. 1. Hydroxyl-Mediated and Direct Electron-Transfer Reactions of Phenol on a Titanium Dioxide-Fluoride System. *Langmuir* **2000**, *16*, 2632–2641.

(23) Minero, C.; Mariella, G.; Maurino, V.; Vione, D.; Pelizzetti, E. Photocatalytic Transformation of Organic Compounds in the Presence of Inorganic Ions. 2. Competitive Reactions of Phenol and Alcohols on a Titanium Dioxide-Fluoride System. *Langmuir* **2000**, *16*, 8964–8972.

(24) Oh, Y.-C.; Bao, Y.; Jenks, W. S. Isotope Studies of Photocatalysis TiO_2-Mediated Degradation of Dimethyl Phenylphosphonate. *J. Photochem. Photobiol. A: Chem.* **2003**, *161*, 69–77.
(25) Park, H.; Choi, W. Effects of TiO_2 Surface Fluorination on Photocatalytic Reactions and Photoelectrochemical Behaviors. *J. Phys. Chem. B* **2004**, *108*, 4086–4093.
(26) Park, J. S.; Choi, W. Enhanced Remote Photocatalytic Oxidation on Surface-Fluorinated TiO_2. *Langmuir* **2004**, *20*, 11523–11527.
(27) Wang, Q.; Chen, C.; Zhao, D.; Ma, W.; Zhao, J. Change of Adsorption Modes of Dyes on Fluorinated TiO_2 and Its Effect on Photocatalytic Degradation of Dyes under Visible Irradiation. *Langmuir* **2008**, *24*, 7338–7345.
(28) Vohra, M. S.; Kim, S.; Choi, W. Effects of Surface Fluorination of TiO_2 on the Photocatalytic Degradation of Tetramethylammonium. *J. Photochem. Photobiol. A: Chem.* **2003**, *160*, 55–60.
(29) Mrowetz, M.; Selli, E. Enhanced Photocatalytic Formation of Hydroxyl Radicals on Fluorinated TiO_2. *Phys. Chem. Chem. Phys.* **2005**, *7*, 1100–1102.
(30) Minella, M.; Faga, M. G.; Maurino, V.; Minero, C.; Pelizzetti, E.; Coluccia, S.; Martra, G. Effect of Fluorination on the Surface Properties of Titania P25 Powder: An FTIR Study. *Langmuir* **2010**, *26*, 2521–2527.
(31) Maurino, V.; Minero, C.; Mariella, G.; Pelizzetti, E. Sustained Production of H_2O_2 on Irradiated TiO_2 – Fluoride Systems. *Chem. Commun.* **2005**, *20*, 2627–2629.
(32) Mino, L.; Pellegrino, F.; Rades, S.; Radnik, J.; Hodoroaba, V. D.; Spoto, G.; Maurino, V.; Martra, G. Beyond Shape Engineering of TiO_2 Nanoparticles: Post-Synthesis Treatment Dependence of Surface Hydration, Hydroxylation, Lewis Acidity and Photocatalytic Activity of TiO_2 Anatase Nanoparticles with Dominant {001} or {101} Facets. *ACS Appl. Nano Mater.* **2018**, *1*, 5355–5365.
(33) Czoska, A. M.; Livraghi, S.; Chiesa, M.; Giamello, E.; Agnoli, S.; Granozzi, G.; Finazzi, E.; Di Valentin, C.; Pacchioni, G. The Nature of Defects in Fluorine-Doped TiO_2. *J. Phys. Chem. C* **2008**, *112*, 8951–8956.
(34) Maheu, C.; Cardenas, L.; Puzenat, E.; Afanasiev, P.; Geantet, C. UPS and UV Spectroscopies Combined to Position the Energy Levels of TiO_2 Anatase and Rutile Nanopowders. *Phys. Chem. Chem. Phys.* **2018**, *20*, 25629–25637.
(35) Achten, C.; Andersson, J. T. Overview of Polycyclic Aromatic Compounds (PAC). *Polycycl. Aromat. Comp.* **2015**, *35*, 177–186.
(36) Neff, J. M.; Anderson, J. W. *Response of Marine Animals to Petroleum and Specific Petroleum Hydrocarbons*, Applied Science Pub., London, **1981**.
(37) Behnajady, M. A.; Eskandarloo, H.; Modirshahla, N.; Shokri, M. Investigation of the Effect of Sol–Gel Synthesis Variables on Structural and Photocatalytic Properties of TiO_2 Nanoparticles. *Desalination* **2011**, *278*, 10–17.
(38) Herrmann, M.; Kaluza, U.; Boehm, H. P. Uber die Chemie der Oberflache des Titandioxids. IV Austausch von Mydroxidionen gegen Fluoridionen. *Z. Anorg. Allg. Chem.* **1970**, *372*, 308–313.

(39) Mueller, R.; Kammler, H. K.; Wegner, K.; Pratsinis, S. E. OH Surface Density of SiO_2 and TiO_2 by Thermogravimetric Analysis. *Langmuir* **2003**, *19*, 160–165.
(40) Kim, J. M.; Chang, S. M.; Kong, S. M.; Kim, K.-S.; Kim, J.; Kim, W.-S. Control of Hydroxyl Group Content in Silica Particle Synthesized by the Sol-Precipitation Process. *Ceram. Int.* **2009**, *35*, 1015–1019.
(41) Kosmulski, M. pH-Dependent Surface Charging and Points of Zero Charge. IV. Update and New Approach. *J. Colloid Interface Sci.* **2009**, *337*, 439–448.
(42) Yu, J. C.; Yu, J.; Ho, W.; Jiang, Z.; Zhang, L. Effects of F^- Doping on the Photocatalytic Activity and Microstructures of Nanocrystalline TiO_2 Powders. *Chem. Mater.* **2002**, *14*, 3808–3816.
(43) Yamaki, T.; Sumita, T.; Yamamoto, S. Formation of $TiO_{2-x}F_x$ Compounds in Fluorine-Implanted TiO_2. *J. Mater. Sci. Lett.* **2002**, *21*, 33–35.
(44) Li, D.; Haneda, H.; Labhsetwar, N. K. Hishita, S.; Ohashi, N. Visible-Light-Driven Photocatalysis on Fluorine-Doped TiO_2 Powders by the Creation of Surface Oxygen Vacancies. *Chem. Phys. Lett.* **2005**, *401*, 579–584.
(45) Yeh, J.; Lindau, I. Atomic Subshell Photoionization Cross Sections and Asymmetry Parameters: $1 \leq Z \leq 103$. *Atomic Data and Nuclear Data Tables* **1985**, *32*, 1–155.
(46) Asahi, R.; Taga, Y.; Mannstadt, W.; Freeman, A. J. Electronic and Optical Properties of Anatase TiO_2. *Phys. Rev. B* **2000**, *61*, 7459–7465.
(47) Sanjinés, R.; Tang, H.; Berger, H.; Gozzo, F.; Margaritondo, G.; Lévy, F. Electronic Structure of Anatase TiO_2 Oxide. *J. Appl. Phys*. **1994**, *75*, 2945–2951.
(48) Di Valentin, C.; Pacchioni, G. Trends in Non-Metal Doping of Anatase TiO_2: B, C, N and F. *Catal. Today* **2013**, *206*, 12–18.
(49) Chen, X.; Burda, C. The Electronic Origin of the Visible-Light Absorption Properties of C-, N- and S-Doped TiO_2 Nanomaterials. *J. Am. Chem. Soc.* **2008**, *130*, 5018–5019.
(50) Henrich, V. E.; Dresselhaus, G.; Zeiger, H. J. Observation of Two-Dimensional Phases Associated with Defect States on the Surface of TiO_2. *Phys. Rev. Lett.* **1976**, *36*, 1335–1339.
(51) Finazzi, E.; Di Valentin, C.; Pacchioni, G. Nature of Ti Interstitials in Reduced Bulk Anatase and Rutile TiO_2. *J. Phys. Chem. C* **2009**, *113*, 3382–3385.
(52) Borodin, A.; Reichling, M. Characterizing TiO_2 (110) Surface States by Their Work Function. *Phys. Chem. Chem. Phys.* **2011**, *13*, 15442–15447.
(53) Nolan, M.; Elliott, S. D.; Mulley, J. S.; Bennett, R. A.; Basham, M.; Mulheran, P. Electronic Structure of Point Defects in Controlled Self-Doping of the TiO_2 (110) Surface: Combined Photoemission Spectroscopy and Density Functional Theory Study. *Phys. Rev. B* **2008**, *77*, 235424.
(54) Roy, A. M.; De, G. C.; Sasmal, N.; Bhattachayya, S. S. Determination of the Flatband Potential of Semiconductor Particles in Suspension by Photovoltage Measurement. *Int. J. Hydrogen Energy* **1995**, *20*, 627–630.
(55) Wardman, P. Reduction Potentials of One-Electron Couples Involving Free Radicals in Aqueous Solution. *J. Phys. Chem. Ref. Data* **1989**, *18*, 1637–1756.

(56) Pellegrino, F.; Morra, E.; Mino, L.; Martra, G.; Chiesa, M.; Maurino, V. Surface and Bulk Distribution of Fluorides and Ti^{3+} Species in TiO_2 Nanosheets: Implications on Charge Carrier Dynamics and Photocatalysis. *J. Phys. Chem. C* **2020**, *124*, 3141−3149.
(57) Kus, M.; Altantzis, T.; Vercauteren, S.; Caretti, I.; Leenaerts, O.; Batenburg, K. J.; Mertens, M.; Meynen, V.; Partoens, B.; Van Doorslaer, S.; Bals, S.; Cool P. Mechanistic Insight into the Photocatalytic Working of Fluorinated Anatase {001} Nanosheets. *J. Phys. Chem. C* **2017**, *121*, 26275-26286.
(58) Gao, H.; Zhang, D.; Yang, M.; Dong, S. Photocatalytic Behavior of Fluorinated Rutile TiO_2(110) Surface: Understanding from the Band Model. *RRL Solar* **2017**, *1*, 1700183.
(59) Lamiel-Garcia, O.; Tosoni, S.; Illas, F. Relative Stability of F-Covered TiO_2 Anatase (101) and (001) Surfaces from Periodic DFT Calculations and ab Initio Atomistic Thermodynamics. *J. Phys. Chem. C* **2014**, *118*, 13667−13673.
(60) Forstmann, F. The Concepts of Surface States. *Prog. Surface Sci.* **1993**, *42*, 21–31.
(61) Lüth, H. *Surfaces and Interfaces of Solid Materials*, 3rd ed., Springer, Berlin, **1995**.
(62) Zhang, Z.; Yates Jr., J. T. Band Bending in Semiconductors: Chemical and Physical Consequences at Surfaces and Interfaces. *Chem. Rev.* **2012**, *112*, 5520−5551.
(63) Shi, J.; Chen, J.; Feng, Z.; Chen, T.; Lian, Y.; Wang, X.; Li, C. Photoluminescence Characteristics of TiO_2 and Their Relationship to the Photoassisted Reaction of Water/Methanol Mixture. *J. Phys. Chem. C* **2007**, *111*, 693–699.
(64) Dozzi, M. V.; D'Andrea, C.; Ohtani, B.; Valentini, G.; Selli, E. Fluorine-Doped TiO_2 Materials: Photocatalytic Activity vs Time-Resolved Photoluminescence. *J. Phys. Chem. C* **2013**, *117*, 25586−25595.
(65) Kohlrausch, R. Theorie des elektrischen Rückstandes in der Leidener Flasche. *Pogg. Ann. Phys. Chem.* **1854**, *91*, 179–214.
(66) Pavesi, L.; Ceschini, M. Stretched-Exponential Decay of the Luminescence in Porous Silicon. *Phys. Rev. B* **1993**, *48*, 17625–17628.
(67) Phillips, J. C. Kohlrausch Relaxation in Electronic and Molecular Glasses. *Chem. Phys.* **1996**, *212*, 41–46.
(68) Greben, M.; Khoroshyy, P.; Liu, X.; Pi, X.; Valenta, J. Fully Radiative Relaxation of Silicon Nanocrystals in Colloidal Ensemble Revealed by Advanced Treatment of Decay Kinetics. *J. Appl. Phys.* **2017**, *122*, 034304.
(69) Brown, S. L.; Krishnan, R.; Elbaradei, A.; Sivaguru, J.; Sibi, M. P.; Hobbie, E. K. Origin of Stretched-Exponential Photoluminescence Relaxation in Size-Separated Silicon Nanocrystals. *AIP Adv.* **2017**, *7*, 055314.
(70) Heger, D.; Nachtigallová, D.; Surman, F.; Krausko, J.; Magyarová, B.; Brumovský, M.; Rubeš, M.; Gladich, I.; Klán, P. *J. Phys. Chem. A* **2011**, *115*, 11412–11422.
(71) Kim, J.-H.; Yonezawa, S.; Takashima, M. Reactivity of Surface Fluorinated TiO_2 and TiAl Particles. In *Modern Synthesis Processes and Reactivity of Fluorinated Compounds*, ed. Groult, H.; Leroux, F. R.; Tressaud, A. Elsevier, Amsterdam, **2017**, chap. 24, pp. 697–717.

(72) Buchalska, M.; Łabuz, P.; Bujak, Ł.; Szewczyk, G.; Sarna, T.; Maćkowski, S.; Macyk, W. New Insight into Singlet Oxygen Generation at Surface Modified Nanocrystalline TiO_2 – the Effect of Near-Infrared Irradiation. *Dalton Trans.* **2013**, *42*, 9468–9475.
(73) Daimon, T.; Nosaka, Y. Formation and Behavior of Singlet Molecular Oxygen in TiO_2 Photocatalysis Studied by Detection of Near-Infrared Phosphorescence. *J. Phys. Chem. C* **2007**, *111*, 4420–4424.

Supporting Information

Surface and Electronic Features of Fluorinated TiO_2 and their Influence on the Photocatalytic Degradation of 1-Methylnaphthalene

Nidhal Fessi,[a,b] Mohamed Faouzi Nsib,[a,g] Luis Cardenas,[c] Chantal Guillard,[c] Frédéric Dappozze,[c] Ammar Houas,[a] Francesco Parrino,[*,d] Leonardo Palmisano,[e] Gilles Ledoux,[f] David Amans,[f] Yves Chevalier[*,b]

[a] Laboratoire de Recherche Catalyse et Matériaux pour l'Environnement et les Procédés (URCMEP, UR11ES85), Faculté des Sciences de Gabès, University of Gabès, Campus Universitaire, Cité Erriadh, 6072 Gabès, Tunisia.

[b] Laboratoire d'Automatique, de Génie des Procédés et de Génie Pharmaceutique (LAGEPP), CNRS UMR 5007, University Claude Bernard Lyon 1, 43 bd 11 Novembre, 69622 Villeurbanne, France.

[c] Institut de Recherches sur la Catalyse et l'Environnement de Lyon (IRCELYON), CNRS UMR 5256, Université Lyon 1, 2 av Albert Einstein, 69626 Villeurbanne, France.

[d] Dipartimento di Ingegneria Industriale, University of Trento, via Sommarive 9, 38123 Trento, Italy.

[e] Department of Engineering, University of Palermo, Viale delle Scienze Ed. 6, 90128 Palermo, Italy.

[f] Université de Lyon, Université Claude Bernard Lyon 1, CNRS, Institut Lumière Matière, 69622 Villeurbanne, France.

[g] Higher School of Sciences and Technology of Hammam Sousse, University of Sousse, Tunisia.

X-ray diffraction. X-ray diffraction patterns of the TiO_2 and TiO_2-F photocatalysts samples were recorded at room temperature by an Ital Structures APD 2000 powder diffractometer using the Cu Kα radiation and a 2θ scan rate of 2 °C·min^{-1}. The angular resolution was 0.055°. The mean crystallite size of the photocatalysts was estimated using the Debye–Scherrer equation:

$$D = 0.9\,\lambda / \beta \cos\theta \qquad \text{(S1)}$$

where D is the mean crystallite size (nm), λ is the wavelength of the X-ray radiation (0.154 nm), θ and β are the diffraction angle and the resolution-corrected width at half height of Bragg reflections.

The diffraction peaks of both the powder patterns of TiO_2 and TiO_2-F (Figure S1) were clearly attributed to the anatase structure of TiO_2 (JCPDS card: 21-1272). In particular, the strong diffraction peaks appearing at 25.28°, 37.81°, 47.99°, 53.95°, 55.0°, 62.9° and 75.0° corresponded to the (101), (004), (200), (105), (211), (204) and (215) crystallographic planes.

The mean crystallite size of TiO_2 nanoparticles calculated using Debye-Scherrer equation (Eq. S1) was about 11 nm. The fluorination process did not change the bulk crystal structure and did not cause any shift in characteristic diffraction peak positions of the anatase structure.

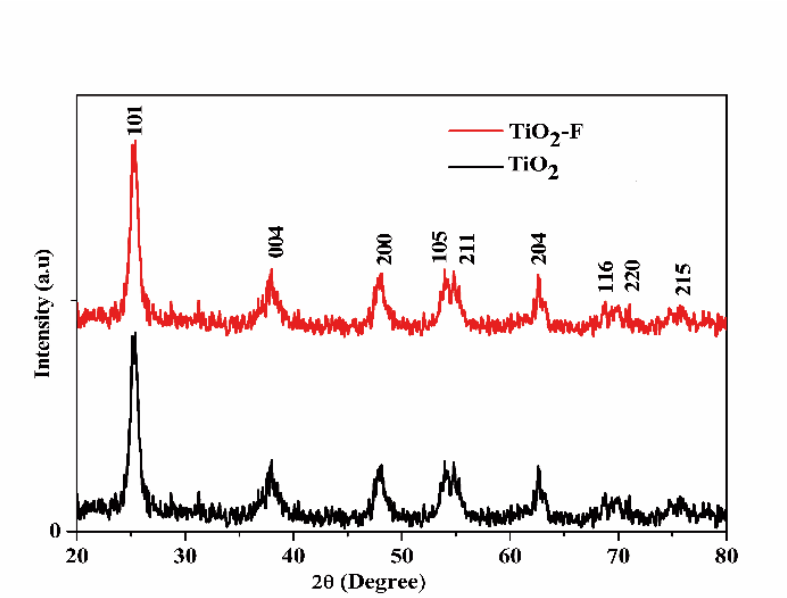

Figure S1. X-ray diffraction patterns of pristine TiO_2 (black line) and TiO_2-F (red line).

Scanning electron microscopy. The morphology of the photocatalyst was examined using a Philips XL30 ESEM scanning electron microscope (SEM), operating at 30 kV on specimens on which a thin layer of gold was deposited. SEM of TiO_2 (Fig. S2) showed aggregates of small elementary nanoparticles. The morphology of elementary nanoparticles was spherical and their surface appeared quite smooth. The size distribution was quite narrow. The particle size appeared quite close to the mean crystallite size calculated by means of XRD patterns. The morphology of TiO_2-F nanoparticles was very similar (not shown).

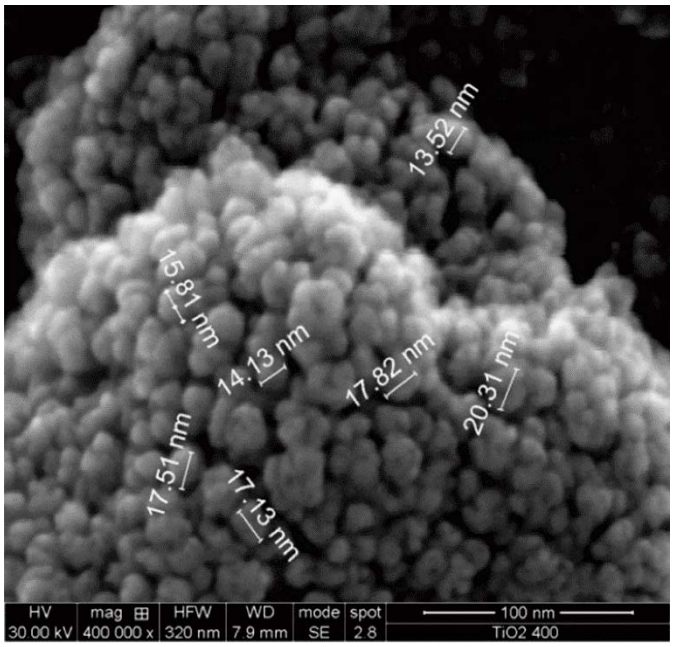

Figure S2. SEM surface morphology of pristine TiO_2.

BET measurements. Nitrogen adsorption and desorption isotherms of the synthesized photocatalysts were measured using a Micrometrics TRISTAR 3000. The specific surface area was assessed using the Brunauer–Emmett–Teller (BET) equation in the relative pressure range p/p_0 between 0.05 and 0.3. Porosity was calculated from the desorption branch above 0.4 relative pressure by the Barrett–Joyner–Halenda (BJH) method. Adsorption and desorption isotherms showed the classical type IV adsorption isotherm suggesting the presence of a mesoporous structure (Figure S3). At high relative pressure from 0.45 to 0.80, the isotherms exhibited a hysteresis loop of type H2, indicating the existence of ink-bottle type pores with narrow necks and wide bodies. The specific surface area calculated using the BET equation was 103 $m^2 \cdot g^{-1}$. Identical results were obtained with TiO_2-F (not shown).

The inset in Figure S3 shows the pore size distribution calculated from the desorption branch of the isotherm using the BJH equation. The pore size distribution of porous volume d*V*/d*D* was narrow and the average pore diameter was about 5 nm.

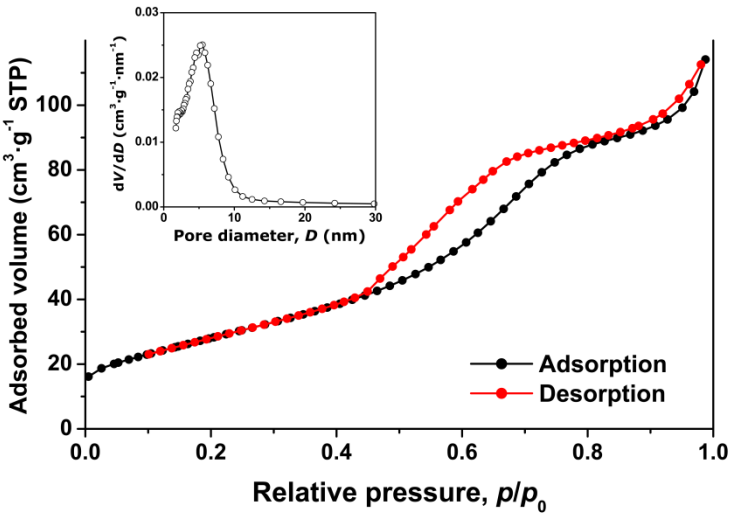

Figure S3. Nitrogen adsorption/desorption isotherms of pristine TiO_2. Inset shows the pore size distribution.

XPS spectra. XPS spectra provided analyses of surface species, namely fluorine bound to titanium atoms and the type of titanium species (Figure S4). The peak corresponding to C 1s at 284.8 eV coming from adventitious carbon of organic contamination was used for the calibration of the energy scale. XPS spectra of TiO_2 and TiO_2-F showed main peaks corresponding to Ti $2p_{3/2}$ at 458.2 eV, Ti $2p_{1/2}$ at 464.0 eV, and O 1s at 529.6 eV. The XPS spectrum of TiO_2-F showed a supplementary F 1s line at 684.3 eV that nicely corresponded to the position of F 1s line of oxyfluoride F–Ti–O group at the surface of fluorine-doped TiO_2 as inferred by several authors.[1–12]

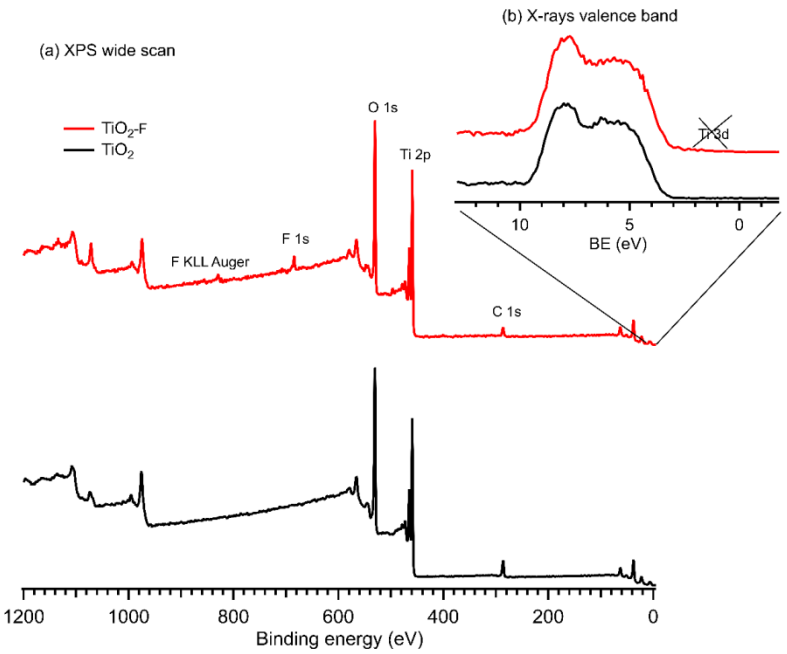

Figure S4. (a) XPS wide spectra of TiO_2 and TiO_2-F. Inset (b) shows the X-rays valence band region. A possible Ti^{3+} 3d state is not visible.

Photoluminescence spectra. Photoluminescence spectra of TiO_2 and TiO_2-F have been recorded at several temperatures between 293 K and 83 K (Figure S5). Photoluminescence progressively increased as a function of decreasing temperature because lesser lattice vibrations at low temperature make the non-radiative decay of the excited states slower. Enhancement of luminescence was stronger at low wavelengths corresponding to radiative deexcitation of electrons trapped in lattice defects of energy between the valence and conduction bands. Whatever the temperature, exciton photoluminescence was not observed. Photoluminescence at low wavelengths was stronger for TiO_2-F than TiO_2, especially at low temperatures where radiative deexcitation is more visible.

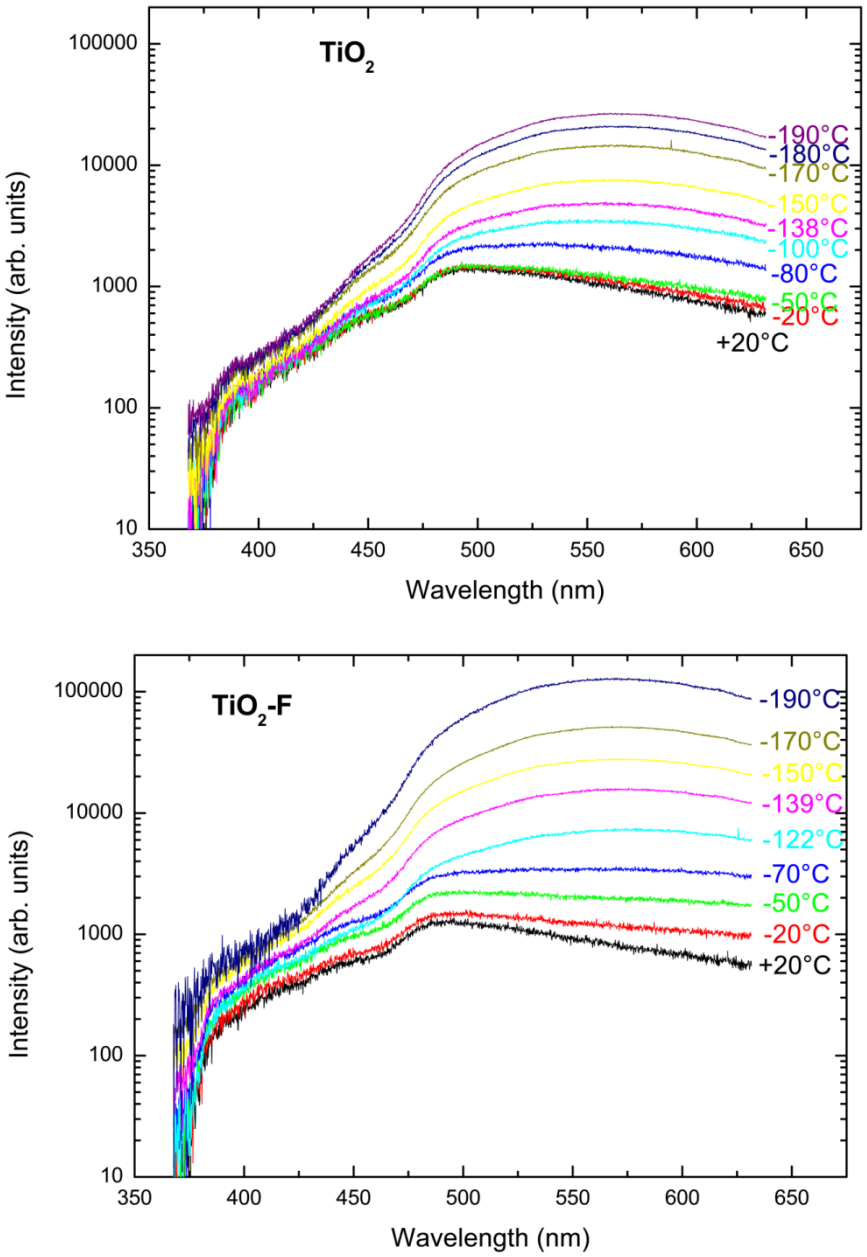

Figure S5. Photoluminescence spectra of TiO_2 and TiO_2-F at different temperatures between 20°C and –190°C.

Photoluminescence decay. Time-resolved photoluminescence at 500 nm showed a non-exponential decay of emitted light. A Kohlrausch stretched exponential decay (Eq. S2) [13,14] was fitted to experimental data.

$$I(t) = I(0)\exp\left(-\left(\frac{t-t_0}{\tau}\right)^{\beta}\right) \quad \text{(S2)}$$

where τ is a time constant, β describes the width of the distribution ($0 \leq \beta \leq 1$), and t_0 is the start time hidden by the excitation pulse. $\beta = 1$ for a single excited state yielding a purely exponential decay. The stretched exponential decay has been often used as a model accounting for the distribution of emission decays [15–18] and also many other relaxation phenomena in disordered media.[19,20] Experimental data was taken for times longer than 10 ns for which the excitation pulse did not perturb emission signal. Adjustment of the three parameters t_0, τ and β (Table S1) yielded a good fit (with R^2 close to 1) over the whole experimental time scale (Fig. S6). For small values of β, the time constant τ does not have a clear physical meaning. The mean lifetime $\bar{\tau}$ of the excited state is estimated as the time when half the energy has been emitted

$$\int_0^{\bar{\tau}} I(t)\, dt = \frac{1}{2}\int_0^{\infty} I(t)\, dt \qquad \text{(S3)}$$

Therefore, a small value of β (broad distribution) can lead to a very small value of the parameter $\bar{\tau}$. Most distributions of excited states yield $0.5 \leq \beta \leq 1$.[15–18,21] The error on $\bar{\tau}$ was estimated as twice the width of the laser light pulse.

The low values of β originated from a broad distribution of deexcitation pathways leading to a broad distribution of exponential decays. Such pathways were predominantly non-radiative because the luminescence intensity was weak. Indeed the mean luminescence decay rate $1/\bar{\tau}$ is defined by contributions to emission of all emitting sites {i} following their own individual lifetime τ_i. For each site {i}, τ_i is a combination of radiative and non-radiative lifetimes:

$$\frac{1}{\tau_i} = \frac{1}{\tau_{i,rad}} + \frac{1}{\tau_{i,non-rad}} \qquad \text{(S4)}$$

Accordingly, the quantum yield equal to the ratio τ/τ_{rad} was low. As a whole, the short non-radiative life-times contribute much to the luminescence decay, even though non-radiative deexcitation does not emit light.

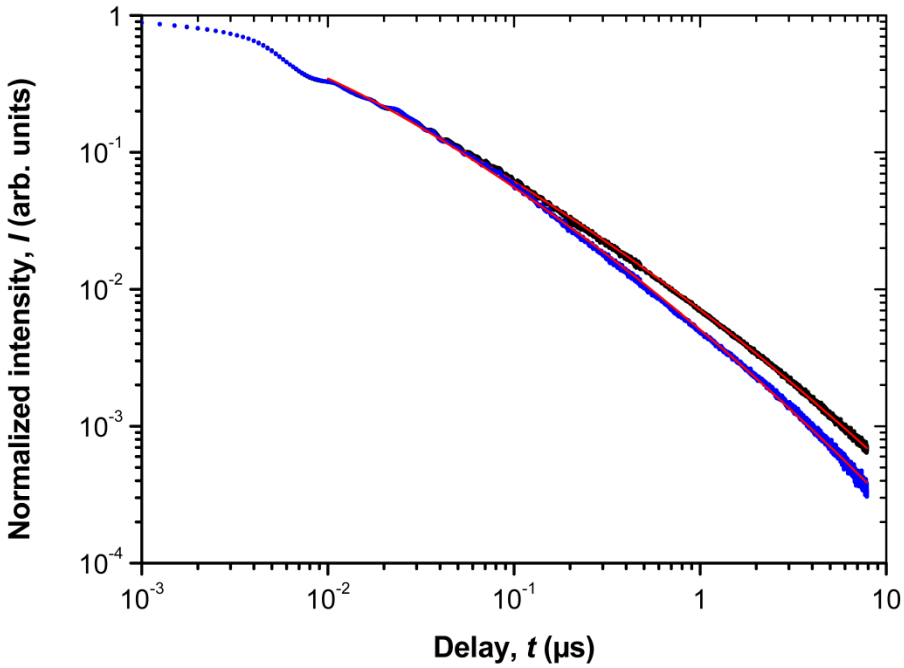

Figure S6. Time-resolved luminescence at 500 nm. Black and blue dots stand for experimental decays of TiO_2 and TiO_2-F respectively. Red lines are the best fits of Eq. S2 to experimental data for delays longer than 10 ns.

	$\bar{\tau}$ (μs)	β	R^2
TiO_2	0.24 ± 0.02	0.081 ± 0.002	0.9986
TiO_2-F	0.13 ± 0.02	0.079 ± 0.002	0.9980

Table S1. Parameters of the best fit of the stretched exponential (Eq. S2) to the time-resolved photoluminescence at 500 nm for delays longer than 10 ns.

References

(1) Fox, M. *Optical Properties of Solids*. *2nd ed, Oxford University Press*, 2010.

(2) Yamaki, T.; Sumita, T.; Yamamoto, S. Formation of $TiO_{2-x}F_x$ Compounds in Fluorine-Implanted TiO_2. *J. Mater. Sci. Lett.* **2002**, *21*, 33–35.

(3) Yu, J. C.; Yu, J.; Ho, W.; Jiang, Z.; Zhang, L. Effects of F^- Doping on the Photocatalytic Activity and Microstructures of Nanocrystalline TiO_2 Powders. *Chem. Mater.* **2002**, *14*, 3808–3816.

(4) Park, H.; Choi, W. Effects of TiO_2 Surface Fluorination on Photocatalytic Reactions and Photoelectrochemical Behaviors. *J. Phys. Chem. B* **2004**, *108*, 4086–4093.

(5) Li, D.; Haneda, H.; Hishita, S.; Ohashi, N.; Labhsetwar, N. K. Fluorine-Doped TiO_2 Powders Prepared by Spray Pyrolysis and Their Improved Photocatalytic Activity for Decomposition of Gas-Phase Acetaldehyde. *J. Fluorine Chem.* **2005**, *126*, 69–77.

(6) Li, D.; Haneda, H.; Labhsetwar, N. K.; Hishita, S.; Ohashi, N. Visible-Light-Driven Photocatalysis on Fluorine-Doped TiO_2 Powders by the Creation of Surface Oxygen Vacancies. *Chem. Phys. Lett.* **2005**, *401*, 579–584.
(7) Li, D.; Haneda, H.; Hishita, S.; Ohashi, N. Visible-Light-Driven N-F-Codoped TiO_2 Photocatalysts. 1. Synthesis by Spray Pyrolysis and Surface Characterization. *Chem. Mater.* **2005**, *17*, 2588–2595.
(8) Ho, W.; Yu, J. C.; Lee, S. Synthesis of Hierarchical Nanoporous F-Doped TiO_2 Spheres with Visible Light Photocatalytic Activity. *Chem. Commun.* **2006**, 1115–1117.
(9) Huang, D.; Liao, S.; Quan, S.; Liu, L.; He, Z.; Wan, J.; Zhou, W. Preparation of Anatase F Doped TiO_2 Sol and Its Performance for Photodegradation of Formaldehyde. *J. Mater. Sci.* **2007**, *42*, 8193–8202.
(10) Wang, Q.; Chen, C.; Zhao, D.; Ma, W.; Zhao, J. Change of Adsorption Modes of Dyes on Fluorinated TiO_2 and Its Effect on Photocatalytic Degradation of Dyes under Visible Irradiation. *Langmuir* **2008**, *24*, 7338–7345.
(11) Pan, J. H.; Zhang, X.; Du, A. J.; Sun, D. D.; Leckie, J. O. Self-Etching Reconstruction of Hierarchically Mesoporous F-TiO_2 Hollow Microspherical Photocatalyst for Concurrent Membrane Water Purifications. *J. Am. Chem. Soc.* **2008**, *130*, 11256–11257.
(12) Sul, Y.-T. Electrochemical Growth Behavior, Surface Properties, and Enhanced *In Vivo* Bone Response of TiO_2 Nanotubes on Microstructured Surfaces of Blasted, Screw-Shaped Titanium Implants. *Int. J. Nanomedicine* **2010**, *5*, 87–100.
(13) Kohlrausch, R. Theorie des elektrischen Rückstandes in der Leidener Flasche. *Pogg. Ann. Phys. Chem.* **1854**, *91*, 179–214.
(14) Phillips, J. C. Kohlrausch Explained: The Solution to a Problem That Is 150 Years Old. *J. Stat. Phys.* **1994**, *77*, 945–947.
(15) Chen, X.; Henderson, B.; O'Donnell, K. P. Luminescence Decay in Disordered Low-Dimensional Semiconductors. *Appl. Phys. Lett.* **1992**, *60*, 2672–2674.
(16) Pavesi, L.; Ceschini, M. Stretched-Exponential Decay of the Luminescence in Porous Silicon. *Phys. Rev. B* **1993**, *48*, 17625–17628.
(17) Greben, M.; Khoroshyy, P.; Liu, X.; Pi, X.; Valenta, J. Fully Radiative Relaxation of Silicon Nanocrystals in Colloidal Ensemble Revealed by Advanced Treatment of Decay Kinetics. *J. Appl. Phys.* **2017**, *122*, 034304.
(18) Brown, S. L.; Krishnan, R.; Elbaradei, A.; Sivaguru, J.; Sibi, M. P.; Hobbie, E. K. Origin of Stretched-Exponential Photoluminescence Relaxation in Size-Separated Silicon Nanocrystals. *AIP Adv.* **2017**, *7*, 055314.
(19) Williams, G.; Watts, D. C. Non-Symmetrical Dielectric Relaxation Behaviour Arising from a Simple Empirical Decay Function. *Trans. Faraday Soc.* **1970**, *66*, 80–85.
(20) Gotze, W.; Sjogren, L. Relaxation Processes in Supercooled Liquids. *Rep. Prog. Phys.* **1992**, *55*, 241–376.
(21) Phillips, J. C. Kohlrausch Relaxation in Electronic and Molecular Glasses. *Chem. Phys.* **1996**, *212*, 41–46.